NONLINEAR FINITE ELEMENT MODELING OF QUARTZ CRYSTAL RESONATORS

By

AUSTIN DALE BEERWINKLE

Bachelor of Science in
Aerospace and Mechanical Engineering
Oklahoma State University
Stillwater, OK, USA
2009

Submitted to the Faculty of the
Graduate College of
Oklahoma State University
in partial fulfillment of
the requirements for
the Degree of
MASTER OF SCIENCE
July, 2011

NONLINEAR FINITE ELEMENT MODELING OF QUARTZ CRYSTAL RESONATORS

Thesis Approved:

Dr. Raman P. Singh

Thesis Advisor

Dr. Jay C. Hanan

Dr. Sandip P. Harimkar

Dr. Mark E. Payton

Dean of the Graduate College

ACKNOWLEDGMENTS

I am pleased to thank my advisor, Dr. Raman P. Singh, for allowing me to be a part of the Mechanics of Advanced Materials Laboratory at Oklahoma State University and affording me the opportunity to work on such an applied project with direct correlations to industry. This link has served to make the current work all the more rewarding. I am indebted to Dr. Goutham R. Kirikera of Geophysical Research Company, LLC (GRC) for his close collaboration throughout the entire project and immense assistance in pointing the way to relevant literature and background studies, without which my understanding of quartz and quartz sensors would not be what it is today, nor would this work be complete. I am grateful to the other student members of MAML for showing me the ropes in graduate school, providing good examples of quality workmanship, and always giving general friendly support through class work and pastimes. Likewise, I must also express gratitude to all the employees of GRC that were welcoming of my attempt to provide what small contribution to their business that I could.

This work was made possible by funding from the Oklahoma Center for Advancement of Science and Technology (OCAST project number AR101-036). My personal inclusion on the project and in graduate school in general was made possible by an initial fellowship sponsored by Conoco-Phillips, assistantships for which I am grateful to the Mechanical and Aerospace Engineering Department, and eventually through the Critical Skills Master's Program as an employee of Sandia National Laboratories. I would like to thank all those at Sandia who made this wonderful opportunity to participate in such a program possible, especially my managers and mentors there

who have remained supportive and engaged even while I have been away from the work site.

Finally, I would not have made it through college, let alone graduate school, if not for the loving encouragement of my parents, Dale and Linda, and the work ethic they instilled in me. I know that their Christian example will continue to be a source of wisdom and sustained strength for me in my own walk with the Savior. Most of all, I appreciate the unwavering support of my new wife to be, Emily, for putting up with the long hours of homework and working at the lab all though my college career, for always being there for me whatever endeavors I have chosen to pursue, and for marrying me even though the time leading up to the wedding has been one of the busiest. I know that attaining this degree will be, to me personally, just one part of the beginning of our new life together.

TABLE OF CONTENTS

LIST OF TABLES

LIST OF FIGURES

CHAPTER 1

INTRODUCTION

1.1 Quartz Crystal Resonators as Temperature and Pressure Sensors

In the past century, the quartz crystal resonator has achieved ubiquitous service in day to day life. From sonar to nanodevices and including most every microchip-enabled product on the market today, the piezoelectric capability of the quartz crystal combined with desirable physical properties make it an irreplaceable component in many electric and electro-mechanical systems. For the majority of these uses, the quartz crystal is employed as a benchmark; a steadfast standard of time-keeping that other components of a system rely on for regulation, stability, and consistency. Therefore, by and large, the body of research on the subject of quartz crystal resonators tends to focus on maintaining this consistency across a range of external factors, such as changing temperature, excessive acceleration, or the presence of induced stresses. Such work seeks to minimize the frequency disturbance caused by inherent nonlinearities within the quartz material as these external factors vary.

By contrast, other applications of the quartz crystal resonator utilize, and in fact rely upon, these nonlinearities to function as sensors for various applications. Since the early 20th century, quartz sensors have been used to measure temperature, pressure, force, acceleration, film thickness, and fluid viscosity among other parameters. Because of their compact size and rugged characteristics combined with excellent sensitivity, resolution and long-term stability, quartz sensors are well suited to serve as down-hole temperature and pressure sensors in oil and gas wells. Despite having a crushing strength of around 2.4 GPa [1] and a Curie point of 573 °C [2], additional

complications that involve a combination of high stress and high temperature limit the performance of quartz in certain sensing applications.

A general picture of what would be described by the term "quartz crystal resonator" is given in Figure 1.1, and is usually nothing more than a thin rectangular or circular quartz plate, although other useful geometries do exist. Visible on each face are the conductive metal electrodes, often gold or copper, that are used to induce an electric field across the quartz domain. An oscillating electric field produces vibrations in the crystal due to the converse piezoelectric effect, as further described in the next chapter. At certain distinct frequencies, these vibrations interact with the boundaries of the quartz geometry to produce standing waves in the crystal, a phenomenon known as resonance. This resonance can control the frequency of a radio transmission, create an acoustic wave in the neighboring fluid, or be measured to deduce pressure or temperature.

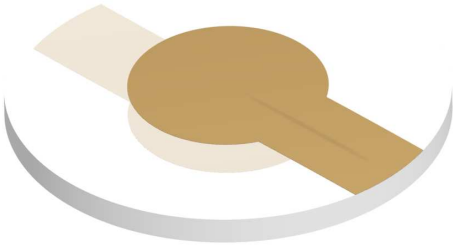

Figure 1.1: Basic round quartz resonator with gold electrodes

1.2 Purpose of Current Work

In spite of the fact that quartz has been used in sensors for more than 100 years, its complete capability has not been fully realized. The primary reason is because of the complex anisotropic and nonlinear nature of its electro-mechanical properties. The goal of the present work is to better understand the interactions of these properties with varying resonator geometry and surroundings, particularly those corresponding

to current uses of quartz resonators as temperature and pressure sensors for the oil and gas industry. To do this first involves developing a multiphysics-based finite element model of quartz that captures the nonlinearity in frequency response associated with changes in pressure and temperature. Secondly, this finite element model is compared to experimental benchmarks in order to propose additions to the currently available constitutive properties of quartz that, if experimentally derived, would enable more accurate simulations.

Ultimately, the developed calibrated model can then be extended to efficiently explore the effect that untested cuts, geometry, and environmental variables have on the output of the sensor (although doing so is not the primary focus of the current work). Accurately modeling the nonlinearities arising in the frequency response of quartz will not only aid in the design of such sensors, but also yield applicable insight into the method of modeling other nonlinear mechanical phenomena involving multiphysics environments, such as for example, those in bio-engineering.

1.3 Notation Used

In the following work, subscripts imply index notation of Cartesian tensors unless otherwise noted, where each index takes on an integer value from 1 to 3, repeated indices imply summation, and indices following commas refer to partial derivatives in the X_1, X_2, and X_3 directions. Superscript θ as in C^{θ}_{ijkl} indicates that a material constitutive variable or tensor is theoretically a function of temperature. Definitions of variables and tensors are provided in context wherever used.

CHAPTER 2

QUARTZ MATERIAL MODEL

2.1 Crystallography of Quartz

The crystal α-quartz, referred to here as simply 'quartz', is one of several distinct crystalline forms of silicon dioxide, SiO_2, or silica, which is one of the most abundant compounds on earth. Many rocks and most sand consist of an amorphous form of silica, yet crystals of α-quartz of high enough quality and size to be used in crystal resonators are much rarer, because defects can severely degrade frequency response and stability. Most high quality naturally occurring crystals are obtained from Brazil. While production of cultured (man-made) quartz from seed crystals serves the majority of industrial uses, quality is critically dependent on growth rate and conditions, such that natural quartz is still preferred for the most stringent applications [2]. Figure 2.1 shows the common natural faces for right-hand quartz, as given in *Dana's Manual of Mineralogy* [3].

The basic chemical building block of quartz crystal is the silicon-oxygen tetrahedron, SiO_4, depicted in Figure 2.2. In quartz, the oxygen atom at each corner of the tetrahedron also serves as a corner of another tetrahedron, such that a series of Si-O-Si bonds link any given tetrahedron to four of its neighbors. The fact that each oxygen atom is used in two separate SiO_4 tetrahedral structures yields the overall chemical formula for quartz, SiO_2.

In the quartz crystal lattice, these pyramidal building blocks are arranged in the form of conjoined helices all pointing in a single direction, known as the optical direction, which has traditionally been drawn pointing vertically in diagrams. Plane

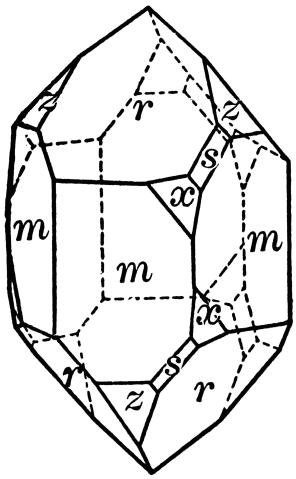

Figure 2.1: Natural crystal faces of quartz [3]

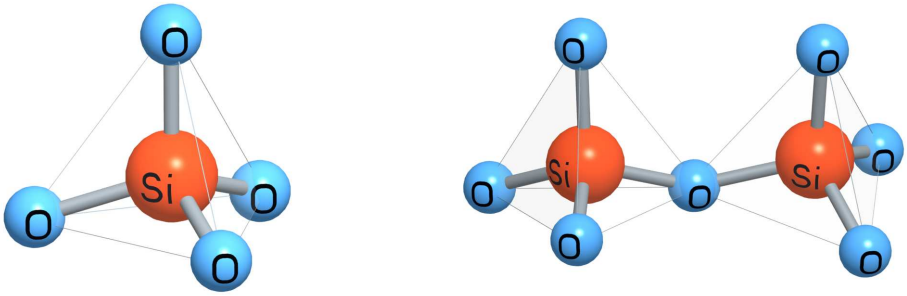

Figure 2.2: Silicon-oxygen tetrahedra

polarized light passing through the crystal in this direction will change its angle of orientation as it passes through the spiraling layers of the quartz lattice. Three tetrahedral layers make up each revolution of the relatively tight 'spiral' in the optical, or c, direction. For this reason, the direction of the optical axis is a direction of three-fold angular symmetry on the macro-scale. It should be noted, however, that this axial symmetry is dispersed throughout the crystal for each conjoined helix, and there is no one single central axis of symmetry on the macro-scale, only rather a *direction* of symmetry. Within the plane normal to the c direction, properties and structure repeat every 120 °, and thus there are three equivalent directions in this plane designated as the a directions as shown in Figure 2.3.

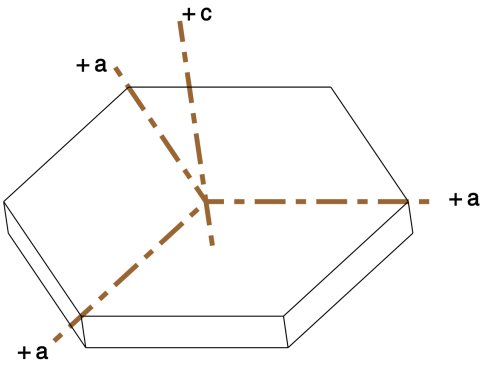

Figure 2.3: Crystallographic axes of quartz

Predictably as for all helical structures, the helices can be of either right- or left-handed form, and both occur naturally in quartz, often in the same crystal growth. This property is called enantiomorphism, and when both the right- and left-hand forms occur together they are known as optical twins (not to be confused with electrical or Dauphiné twins which occur due to a certain kind of dislocation in the lattice of a crystal of single-handedness).

2.2 From Crystal to Engineering Material

While quartz, as a crystal, has been recognized since antiquity and studied scientifically since the origins of crystallography around the 17th century, the understanding of quartz in its current use as an engineering material has its roots in Jacques and Pierre Curie's discovery of piezoelectricity in 1880. Namely, the Curie brothers observed the piezoelectric effect in that applying pressure to quartz produced a voltage. They then later also observed the converse piezoelectric effect, applying voltage made the crystal deform. Besides being used in some lab equipment that would later prove useful for Pierre and his wife Marie during their more famous work with radioactivity, the brothers' discovery was shelved until a few years prior to when Walter Guyton Cady invented the first quartz crystal oscillator in 1921. Originally employed in sonar and radio frequency standards, by World War II such resonators were in wide-scale

production, playing a critical role in the developmental explosion in telecommunications equipment [4]. The pervasion of the microchip into recent times forms another widespread application area for the quartz crystal resonator, where it is used to quantize the timing of the internal functions of the chip. Obviously with such broad use, many have contributed to the science behind the quartz resonator. The direct contributions to the current work, in the form of material data that serve as input to the finite element model, are given in Section 2.5.

Interestingly, given the widespread use of its fruits, the scientific field of piezoelectricity has been surprisingly disjointed at times, a tendency which continues today in some respects. Even as early as 1946, Cady recognized in his comprehensive book *Piezoelectricity* a troubling trend within the archive of experimental quartz articles:

> Through the voluminous literature on the properties of quartz crystals there runs, like a crack in an otherwise clear crystal, an amazing ambiguity concerning the distinction between right- and left-quartz, the positive sense of the directions of the X- and Y- axes, and the positive sense of the angles of rotation. [1]

Since this time, the organizations that govern the standards, notably the Institute of Radio Engineers (IRE) which later merged to become the Institute of Electrical and Electronics Engineers (IEEE), have found themselves on both sides of the fence with new revisions that directly contradict older standards. Indeed, a reader today is not hard-pressed to find publications that mix the conflicting conventions of previous authors between their figures, material data, and references, even within a single document. Still, most literature in use today can be traced to one of two conventions: *IEEE Std 176-1949* or *IEEE Std 176-1987*. The former was adopted from the IRE standard when the IEEE was formed in 1963 (not to be confused with the 1945 IRE standard it replaced), while the latter is to date the most recent IEEE ruling on the subject.

The fundamental difference between these two conventions from 1987 and 1949 is the definition of the theoretical right-handed X-Y-Z Cartesian coordinate system relative to the physical structure of the quartz crystal lattice [5]. For right-handed quartz, the Cartesian coordinate system in *IEEE Std 176-1987* is rotated 180 ° about the Z-axis (or, unanimously, the optical axis) from the coordinate system used in *IEEE Std 176-1949*. This amounts to an inversion of the "positive sense of the directions of the X- and Y- axis" to which Cady referred, and has broad implications for defining signs of material properties and cut angles.

One such consequence is illustrated in Figure 2.4 regarding the differing definition of cut plates of quartz. Such definitions are of great importance, since the anisotropy of quartz combined with the high sensitivity of the resonator dictates that any geometry must be exactingly described relative to the crystal matrix itself (even simple plates). Note both the conventions mentioned use the same logic to define a type of cut *after* a Cartesian coordinate system has been established in the lattice.

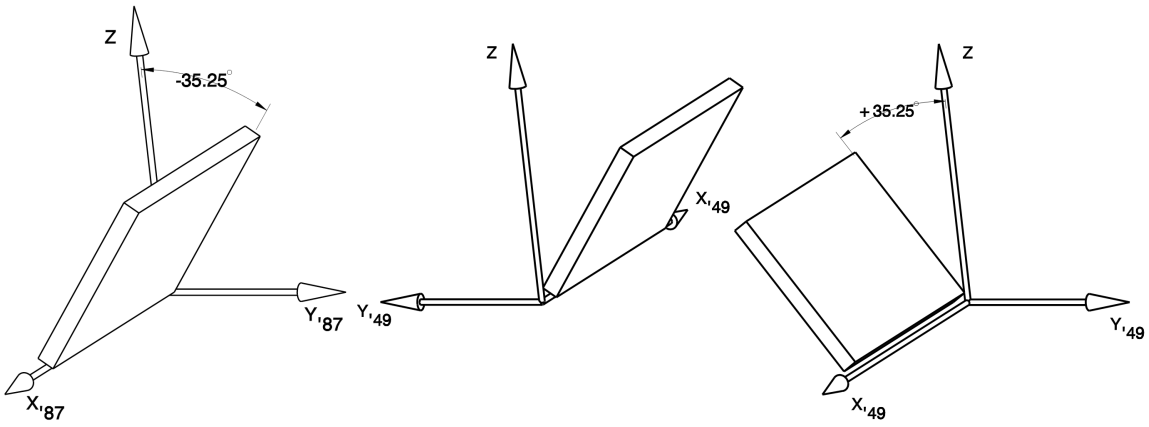

(a) IEEE Std 176-1987 $(YXl) -35.25\,^\circ$

(b) IEEE Std 176-1949 $(YXl) 35.25\,^\circ$ (two views from opposite directions)

Figure 2.4: Comparing conventions for the definition of the AT-Cut

Namely the full definition involves, at most, five letters followed by three numbers. The first two letters call out the cardinal direction (X, Y, or Z) of the thickness and length (that is the shortest and longest dimensions), respectively, of the theoretical

rectangular plate used as a starting point. For instance, YX is a common basis for denoting the Y-Cut family, which includes the AT-, BT-, CT-, and DT-Cuts. YX denotes a rectangular plate on the X-Z plane (with its thickness or normal vector in the Y-direction) of which the X dimension is the longest (thus designated the 'length'). The next three letters (if needed) denote the axes used for consecutive rotations of the basis geometry about the length, width and thickness directions (l, w, and t) in any desired order. The final numbers directly correspond to the previous l, w, or t letters and display, in order, the magnitude of rotation angle for each axis denoted, with positive sign according to the right-hand rotation rule. See either the 1987 convention [5] or the 1949 convention [6] for further examples. Note that three rotations are the maximum needed to describe any general three-dimensional orientation of the plate, and less can be used if possible. This method of three rotations is compatible with the familiar concept of Euler angles. Note that most finite element programs, however, do not use this logic of defining the geometry relative to the material coordinate system, and so additional care must be taken when material orientation is defined in the context of finite element software.

Although the differing coordinate system conventions amount to a simple change of sign for the AT-Cut definition, the effect on the coordinate transformation of, for example, the third-order tensor describing piezoelectric coupling or the sixth-order tensor of nonlinear elastic coefficients, is somewhat more subtle and prone to error, especially if doubly rotated cuts are considered. For this reason, the current work will seek to preserve the convention of the majority of the used material data as referenced, which happens to be in line with the earlier *IEEE Std 176-1949*, as is common in current literature. The AT-Cut defined relative to this material data used is a $+35.25\,^\circ$ rotation of the Y-Cut about the $+X$-axis as shown in Figure 2.4(b). The reader interested in further details of the convention differences present in early quartz works and piezoelectric standards is referred to a concise review by T.R. Meeker [7].

Not surprisingly, the most recent IEEE Standard on Piezoelectricity *IEEE Std 176-1987* was formally withdrawn on March 6, 2000, and the IEEE does not currently endorse any subsequent piezoelectric standard whatsoever.

2.3 Piezoelectricity

Let us now take a closer look at the physics of piezoelectricity that will be needed to form the foundation of the finite element model. The prefix piezo- is derived from the Greek word meaning to press or squeeze, so piezoelectricity could easily be translated as 'pressure electricity'. As previously described, the Curie brothers first observed that applying pressure to quartz (and other crystals such as Rochelle salt) produced an electric voltage. This phenomenon is known as the piezoelectric effect. Similarly there exists the converse piezoelectric effect: applying voltage makes the crystal deform. Both scenarios can be described as a coupling of basic mechanical and electrical responses, and it is advantageous to first consider only the linear one-dimensional forms of each.

$$T = CS \tag{2.1}$$

$$D = \epsilon E \tag{2.2}$$

Equation (2.1) is easily recognized as Hooke's Law, where T is stress in pascals, S is strain in meters per meter, and C is Young's Modulus or stiffness also in pascals. This equation governs deformation via strains. Equation (2.2) is an electrostatic equation defining the electric displacement, D, using electric field E, and total dielectric permittivity ϵ (in respective units of coulombs per square meter, volts per meter, and farads per meter). This equation governs the voltage via the electric field. This quasistatic, rather than dynamic, electric formulation is a valid assumption because the phase velocities of acoustic waves are approximately five orders of magnitude less than the velocities of electromagnetic waves [5]. Electric displacement is not technically a

pure displacement field as would initially be assumed, as shown in another definition:

$$D = \epsilon_0 E + P \tag{2.3}$$

Equation (2.3) shows D as the addition of a displacement field P, and a non-displacement field $\epsilon_0 E$. Here ϵ_0 is free space permittivity and P is the real displacement of charges within a material to form dipoles normalized per unit volume (polarization density). Equations (2.2) and (2.3) are equivalent assuming linear proportional response of polarization to the electric field.

Equations (2.1) and (2.2) describe two unrelated physical behaviors for most materials, but for piezoelectric materials such as quartz, the two cannot be separated. The reactions are coupled, so one should expect that some terms from each will be mixed together. Again assuming linearity but expanding our definition to three dimensions, the stress-charge form of the linear piezoelectric equations [5] is:

$$T_{ij} = C^E_{ijkl} S_{kl} - e_{kij} E_k \tag{2.4}$$

$$D_i = e_{ikl} S_{kl} + \epsilon^S_{ij} E_j \tag{2.5}$$

Note the new piezoelectric constant, or coupling tensor, e that appears in both equations. The coupling tensor has units of farads per meter, and it is this material property that defines the extent of the coupling in piezoelectric materials. The higher the value, the more voltage induced for a given applied mechanical strain. Also the new superscripts for c^E and ϵ^S indicate that these material properties are measured at zero or constant electric field and strain, respectively, because again the two responses cannot be assumed to be independent of one another.

As qualitative example of the piezoelectric effect [2], consider the hypothetical differential material element commonly referred to in mechanical engineering courses, except now the element has an internal distribution of positive and negative charges, as shown in Figure 2.5. There are some states of strain that will induce an electric dipole in the element. The direction of the dipole would depend on the direction

of the strain, and would be zero at zero strain because the charges are then equally distributed. Likewise the piezoelectric effect in quartz can be related to the displacement of charged ions in the crystal lattice, except of course with a complex three-dimensional structure.

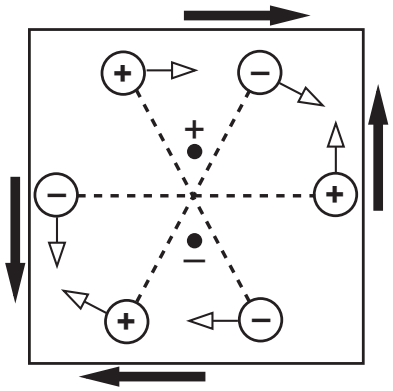

Figure 2.5: Hypothetical piezoelectric effect of an element in shear [2]

2.4 Thermoelastic Definition of Quartz

With a material Cartesian coordinate system previously established together with the anisotropic symmetry of quartz provided by the crystal structure, one has a backdrop for a brief review of some general thermoelastic definitions that are employed throughout the current work. The following is meant to setup only those definitions used for the current mechanical model including stress, strain, displacement, and motion. For further investigation into the continuum mechanics of materials, the reader is directed to one of the many textbooks available on the subject, for instance *Elasticity* by Martin H. Sadd [8] or *Introduction to the Mechanics of a Continuous Medium* by Lawrence E. Malvern [9].

Before trying to define a jumping off point, first let us logically consider the possibilities for material models that can be used to describe the state of quartz. Recalling the exacting uses of quartz sensors together with crystallographic considerations previously covered, one knows that our material model will need to be

anisotropic, temperature dependent, and able to accurately describe the vibrations of the quartz resonator even under changing temperature and pressure. The common linear isotropic material model that is used in educational exercises and analyses of some metals fails on all counts. Long term time dependent effects, such as hysteresis, stress relaxation, and resonator aging, are not of interest in this study, so any elasto-plastic models can be ruled out. The same goes for frictional losses and dampening, which are not examined in this study. Knowing the material properties of quartz are nonlinear coupled with the sensors being exposed to high temperatures and pressures, one can hypothesize that secondary strain effects from large deformations may be non-negligible.

After applying these considerations, one should expect to aim for an anisotropic, nonlinear, temperature dependent material model that does not assume small deformations. The remaining question is to the degree of nonlinearity considered, since any arbitrarily high degree can be used for a nonlinear stress-strain relation. As it turns out, the nonlinearity of our model is limited in this regard by the known material properties of quartz, which are only the lowest two degrees possible. These known properties, the second- and third-order elastic coefficients (so named for their compressed-form tensor order), are later found to be mostly sufficient. Thus the nonlinear governing equations of thermoelasticity in Lagrangian formulation are used as the base material model, where U_i is displacement, S_{ij} is the Lagrangian strain tensor, T_{ij} is the second Piola-Kirchhoff stress tensor, P_i is the surface traction, "in V" marks the differential equation of motion for the domain volume, and "on S" marks the boundary condition on the surfaces with normal vector n_i. Other variables contain material parameters, such as C^{θ}_{ijkl} and C^{θ}_{ijklmn} for second- and third-order stiffness coefficients and λ^{θ}_{ij} for the stress coefficients of temperature, and are defined in the next section (§2.5). These relations are similar to those given by Lee and

Yong [10] except that the degree of nonlinearity was limited as previously described.

$$S_{ij} = \tfrac{1}{2}\left(U_{j,i} + U_{i,j} + U_{k,i}U_{k,j}\right) \tag{2.6}$$

$$T_{ij} = C^{\theta}_{ijkl}S_{kl} + \tfrac{1}{2}C^{\theta}_{ijklmn}S_{kl}S_{mn} - \lambda^{\theta}_{ij} \tag{2.7}$$

$$\rho_0\ddot{U}_i = \left(T_{ij} + T_{jk}U_{i,k}\right)_{,j} \text{ in V} \tag{2.8}$$

$$P_i = n_j(T_{ij} + T_{jk}U_{i,k}) \text{ on S} \tag{2.9}$$

Theoretically, modifying the Hooke's Law portion of the simplistic linear piezoelectric model in Section 2.3 with the nonlinear Equation (2.7) (used along with the other definitions for the model in Equations (2.6) through (2.9)), together with Gauss's Law for an insulator as the electrical governing differential equation, Equation (2.10), gives a complete picture of what is to be solved in order to fully model both the response of quartz to external temperature and pressure as well as the frequency response, all simultaneously in a single step.

$$D_{i,i} = 0 \text{ in V} \tag{2.10}$$

Such a model would relate the so-called *natural* state of the quartz (stress free at reference temperature) directly to the *final* state, these two states being as illustrated in Figure 2.6. Fortunately, a further simplification is suggested by Lee and Yong [10]. Based on the valid assumption that the frequency response involves only small deformation, Lee and Yong suggest the problem can be divided into two steps known as the *initial* and *incremental* parts. These two steps link between three distinct sequential states of the quartz resonator: the natural state, the *initial* state (also called the intermediate state in other publications [11]), and the final state. By using the Lagrangian formulation, the displacements of all three states are referred to a single reference frame corresponding to the unstressed natural state. This is illustrated in Figure 2.6 which is derived from similar figures by Lee and Yong [10][12] and Yong and Wei [11].

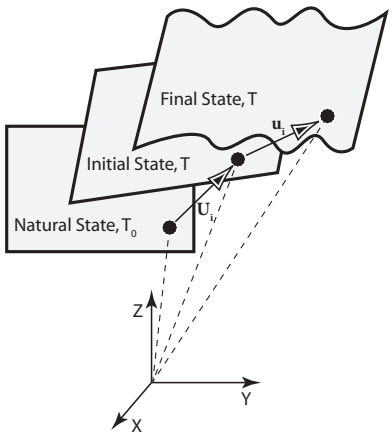

Figure 2.6: The three states of the initial-incremental thermoelastic model [10]

The initial response is modeled using nonlinear equations of the form previously given in Equations (2.6) through (2.9). The initial model solves for the displacement, strain, and stress due to external factors like pressure loading and temperature changes. It does not, however, contain the frequency response due to piezoelectrically driven vibrations, so no piezoelectric factors are included in the initial model. It is, in that respect, a somewhat more traditional solid mechanics formulation. The incremental response, on the other hand, includes only the displacement, strain, and stress of these piezoelectric vibrations, and no external loads. It uses linear (but still temperature dependent) strain and stress definitions, because incremental deformations are assumed to be small. The final state is then defined as the superposition of the *initial* response and the *incremental* response.

Knowing the form of the governing equations for the initial model, which must be the same nonlinear form as the governing equations for the direct model previously defined (Equations (2.6) through (2.9)), the incremental governing equations can be derived from subtracting the initial equations from the direct equations and then applying the small deformation assumptions to eliminate any nonlinearity. This derivation is performed by Lee and Yong [10], the results of which are Equations (2.11) through (2.14). (The degree of nonlinear terms was limited here to only the highest

degree used in this study, which corresponds to the limit of currently available quartz material data.)

$$s_{ij} = \tfrac{1}{2}\left(u_{j,i} + u_{i,j} + U_{k,j}u_{k,i} + U_{k,i}u_{k,j}\right) \tag{2.11}$$

$$t_{ij} = (C^{\theta}_{ijkl} + C^{\theta}_{ijklmn}S_{mn})s_{kl} \tag{2.12}$$

$$\rho_0 \ddot{u}_i = \left(t_{ij} + t_{jk}U_{i,k} + T_{jk}u_{i,k}\right)_{,j} \text{ in V} \tag{2.13}$$

$$p_i = n_j(t_{ij} + t_{jk}U_{i,k} + T_{jk}u_{i,k}) \text{ on S} \tag{2.14}$$

With this mechanical definition, and the addition of temperature dependence to the permittivity and coupling tensors, the overall stress-strain piezoelectric formulation becomes (where the newly derived Equation (2.12) is substituted in Equation (2.4) for Hooke's Law):

$$t_{ij} = (C^{\theta}_{ijkl} + C^{\theta}_{ijklmn}S_{mn})s_{kl} - e^{\theta}_{kij}E_k \tag{2.15}$$

$$D_i = e^{\theta}_{ikl}s_{kl} + \epsilon^{\theta}_{ij}E_k \tag{2.16}$$

Here the capitalized variables U_i, S_{ij}, and T_{ij} are initial model values as previously defined, while lower case variables u_i, s_{ij}, and t_{ij} are the linear incremental displacement, strain, and stress, respectively to be solved for with these equations. It can be seen that the three initial fields $U_{i,j}$, S_{ij}, and T_{ij} will affect the incremental response, and thus also affect the frequency response of the quartz model. This is a very important observation, because it directly defines the logical sequence of the finite element model. Namely the initial model must be solved first in order to find $U_{i,j}$, S_{ij}, and T_{ij}, which are then plugged in to the incremental model as field constants. Finally, the linear incremental model can be solved to find the desired frequency response along with the associated u_i, s_{ij}, and t_{ij}.

2.5 Constitutive Quartz Material Properties

With the equations for the two-step material model in hand, the final piece of the puzzle before these equations can be used in a finite element model is the numerical

definition of those quartz material properties which are present in the governing equations. Due to the wide range of temperatures that the finite element model will seek to describe, it is advantageous to define the constitutive attributes as functions of temperature, so that the model will always be provided with the most realistic input possible. This is achieved using the concepts of Taylor series and power series approximations of various degrees along with temperature derivatives as follows, first for the second-order elastic coefficient, C^{θ}_{ijkl} [12][13].

$$C^{\theta}_{ijkl} = C_{ijkl} + C^{(1)}_{ijkl} \cdot \theta + \tfrac{1}{2} C^{(2)}_{ijkl} \cdot \theta^2 + \tfrac{1}{6} C^{(3)}_{ijkl} \cdot \theta^3 \tag{2.17}$$

Where θ is the temperature difference defined by $\theta = T - T_{\text{ref}}$ (T_{ref} is usually 25 °C) and the temperature derivatives are defined by:

$$C^{(n)}_{ijkl} = \frac{\partial^{(n)} C_{ijkl}}{\partial T^n} \qquad n = 1,\ 2,\ 3$$

Similarly, for the temperature dependence of the third-order elastic coefficient:

$$C^{\theta}_{ijklmn} = C_{ijklmn} + C^{(1)}_{ijklmn} \cdot \theta + \tfrac{1}{2} C^{(2)}_{ijklmn} \cdot \theta^2 \tag{2.18}$$

Where:

$$C^{(n)}_{ijklmn} = \frac{\partial^{(n)} C_{ijklmn}}{\partial T^n} \qquad n = 1,\ 2$$

Generally, the linear thermal expansion coefficients are measured and available instead of the stress coefficients of temperature, λ^{θ}_{ij}, where an approximate relationship exists between the two using thermal strains, α^{θ}_{ij}, that can be assumed of the form:

$$\lambda^{\theta}_{ij} \approx C^{\theta}_{ijkl} \alpha^{\theta}_{kl} + \tfrac{1}{2} C^{\theta}_{ijklmn} \alpha^{\theta}_{kl} \alpha^{\theta}_{mn} \tag{2.19}$$

So then the thermal strains, α^{θ}_{ij}, are defined by:

$$\alpha^{\theta}_{ij} = \alpha^{(1)}_{ij} \cdot \theta + \alpha^{(2)}_{ij} \cdot \theta^2 + \alpha^{(3)}_{ij} \cdot \theta^3 \tag{2.20}$$

Where $\alpha^{(1)}_{ij}$, $\alpha^{(2)}_{ij}$, and $\alpha^{(3)}_{ij}$ are the first-, second-, and third-order thermal expansion coefficients, respectively.

As far as the electrical properties are concerned, the temperature dependence of the piezoelectric coupling tesnsor e^{θ}_{ijk} and the dielectric permittivity $\varepsilon^{\theta}_{ijk}$ can be defined as power series:

$$e^{\theta}_{ijk} = e_{ijk} + e^{(1)}_{ijk} \cdot \theta + e^{(2)}_{ijk} \cdot \theta^2 + e^{(3)}_{ijk} \cdot \theta^3 \tag{2.21}$$

$$\varepsilon^{\theta}_{ij} = \varepsilon_{ij} + \varepsilon^{(1)}_{ij} \cdot \theta + \varepsilon^{(2)}_{ij} \cdot \theta^2 + \varepsilon^{(3)}_{ij} \cdot \theta^3 \tag{2.22}$$

Here, $e^{(1)}_{ijk}$ represents the first-order thermo-piezoelectric constants, $e^{(2)}_{ijk}$ represents the second-order thermo-piezoelectric constants, et cetera. Then also $\varepsilon^{(1)}_{ij}$ stands for the first-order thermo-dielectric constants, $\varepsilon^{(2)}_{ij}$ the second-order thermo-dielectric constants, et cetera.

Many scientists and engineers over the years (like for instance Yong and Wei [11]) have contributed to the vast task of defining all of these separate constitutive properties as a function of temperature, even after the initial work to define the properties at a single temperature. Due to the nonlinear nature of the temperature dependence and the nonlinearity of the governing equations themselves, often studies for new material constants must necessarily take into account the previous more basic values, such that the entire body of work for quartz properties is truly foundational to our current understanding. With this in mind, the following Table 2.1 defines the immediate sources of material data for this study, used exactly as they appear in the relations described above (except for total thermoelastic stiffnesses discussed at the end of this section). Most of these data were also previously compiled in the doctoral dissertation of Mihir Patel [14], which greatly aided in the current compilation. Note that Patel's appendix uses the abbreviated engineering notation, or Voigt notation, to report the numerical values of tensors for brevity, which does not change any numerical values themselves. A comparison between this notation and the formal tensor notation used previously to express calculations was given by Brugger [15].

Note that the temperature derivatives of the third-order elastic stiffness coefficients

Symbol	Property	Reference
C_{ijkl}	2nd-Order Elastic Stiffness	Bechmann, et al. (1962) [16]
$C^{(1)}_{ijkl}$	1st Temperature Derivative of 2nd-Order Elastic Stiffness	Lee, Yong (1986) [12]
$\tilde{C}^{(2)}_{ijkl}$	Effective 2nd Temp. Deriv. of 2nd-Order Elastic Stiffness	Lee, Yong (1986) [12]
$\tilde{C}^{(3)}_{ijkl}$	Effective 3rd Temp. Deriv. of 2nd-Order Elastic Stiffness	Lee, Yong (1986) [12]
C_{ijklmn}	3rd-Order Elastic Stiffness	Thurston, et al. (1966) [17]
$C^{(1)}_{ijklmn}$	1st Temperature Derivative of 3rd-Order Elastic Stiffness	[Not Available]
$C^{(2)}_{ijklmn}$	2nd Temperature Derivative of 3rd-Order Elastic Stiffness	[Not Available]
$\alpha^{(1)}_{ij}$	1st-Order Thermal Expansion Coefficient	Bechmann, et al. (1962) [16]
$\alpha^{(2)}_{ij}$	2nd-Order Thermal Expansion Coefficient	Bechmann, et al. (1962) [16]
$\alpha^{(3)}_{ij}$	3rd-Order Thermal Expansion Coefficient	Bechmann, et al. (1962) [16]
e_{ijk}	Piezoelectric Constants	Bechmann (1958) [18]
$e^{(1)}_{ijk}$	1st-Order Thermo-Piezoelectric Constants	Yong, Wei (2000) [11]
$e^{(2)}_{ijk}$	2nd-Order Thermo-Piezoelectric Constants	Yong, Wei (2000) [11]
$e^{(3)}_{ijk}$	3rd-Order Thermo-Piezoelectric Constants	Yong, Wei (2000) [11]
ε_{ij}	Dielectric Constants	Bechmann (1958) [18]
$\varepsilon^{(1)}_{ij}$	1st-Order Thermo-Dielectric Constants	Yong, Wei (2000) [11]
$\varepsilon^{(2)}_{ij}$	2nd-Order Thermo-Dielectric Constants	Yong, Wei (2000) [11]
$\varepsilon^{(3)}_{ij}$	3rd-Order Thermo-Dielectric Constants	Yong, Wei (2000) [11]
$D^{(1)}_{ijkl}$	1st-Order Total Thermoelastic Stiffness †	Yong, Wei (2000) [11]
$D^{(2)}_{ijkl}$	2nd-Order Total Thermoelastic Stiffness †	Yong, Wei (2000) [11]
$D^{(3)}_{ijkl}$	3rd-Order Total Thermoelastic Stiffness †	Yong, Wei (2000) [11]

† intended use for stress-free models only

Table 2.1: References for the constitutive material properties used as inputs

are not available in current literature. Therefore, the nonlinear stiffness of the model in its present state is independent of temperature, and Equation (2.18) in the standard material definition is effectively reduced to simply:

$$C^{\theta}_{ijklmn} = C_{ijklmn} \tag{2.23}$$

Part of the purpose of the present work is to better define the role of these unknown temperature derivatives in accurately predicting the frequency response of temperature and pressure sensors.

Also of note is the 'effective' modification for the second and third temperature derivatives of second-order elastic stiffness, as given by Lee and Yong [12] in 1986. This is because (in the method of derivation they used) the actual derivatives' values are intimately tied to the unknown temperature derivatives of nonlinear elastic stiffnesses (third-order elastic stiffness and above) such that one must assume a stress-free thermal expansion for the initial strain in order to accurately use the values given. This can be seen in their theoretical definition where, again for simplicity, the maximum order of nonlinearity is restricted to the third-order elastic constants rather than the fourth- and fifth-order which are included in the referred source:

$$\tilde{C}^{(2)}_{ijkl} = C^{(2)}_{ijkl} + 2C^{(1)}_{ijklmn}\alpha^{(1)}_{mn} \tag{2.24}$$

$$\tilde{C}^{(3)}_{ijkl} = C^{(3)}_{ijkl} + 6C^{(1)}_{ijklmn}\alpha^{(2)}_{mn} + 3C^{(2)}_{ijklmn}\alpha^{(1)}_{mn} \tag{2.25}$$

Equations (2.24) and (2.25) show the inherent dependence of $\tilde{C}^{(2)}_{ijkl}$ and $\tilde{C}^{(3)}_{ijkl}$ on the unknown temperature derivatives of the third-order elastic stiffness, $C^{(1)}_{ijklmn}$ and $C^{(2)}_{ijklmn}$, where pure thermal strains must be assumed as the acting initial strains in the nonlinear terms. This discrepancy does not change their use in Equation (2.17) where $\tilde{C}^{(2)}_{ijkl}$ and $\tilde{C}^{(3)}_{ijkl}$ are to be used in place of $C^{(2)}_{ijkl}$ and $C^{(3)}_{ijkl}$, but does however affect their accuracy when stresses are applied at temperature. Still they represent the best scenario available, and are essential to what reasonable amount of accuracy is seen in the current model.

In fact, the effective second and third temperature derivatives of second-order elastic stiffness were revisited by Yong and Wei [11] in 2000. The derivation was updated to include piezoelectric effects which had previously been neglected, which yielded only minor (generally less than 1%) changes from the Lee and Yong values [13] [12]. Their final results were not, however, fully reduced to the more basic effective second and third temperature derivatives of second-order elastic stiffness, but used to derive what the authors called the "temperature derivatives of elastic stiffnesses," or in the current work referred to as "total thermoelastic stiffness" for disambiguation. These total thermoelastic stiffnesses actually inherently include the temperature dependency of each second-, third-, and higher-order stiffness term (thus eliminating the need to denote them as 'effective'). This formulation is only useful for describing the incremental stiffness in stress-free thermal expansion.

Applying it involves a different incremental stress-strain relation than previously provided, but in the end gives a more direct calculation for the incremental stiffness as a third-order polynomial function of temperature assuming a stress-free state. Namely, the incremental stress-strain Equation (2.12) and all subsequent definitions for C^{θ}_{ijkl} and C^{θ}_{ijklmn} are replaced by the following single equation:

$$t_{ij} = (C_{ijkl} + D^{(1)}_{ijkl} \cdot \theta + D^{(2)}_{ijkl} \cdot \theta^2 + D^{(3)}_{ijkl} \cdot \theta^3)s_{kl} \tag{2.26}$$

Likewise, the overall incremental piezoelectric governing Equation (2.15) that is derived from Equation (2.12) must be similarly modified, as in:

$$t_{ij} = (C_{ijkl} + D^{(1)}_{ijkl} \cdot \theta + D^{(2)}_{ijkl} \cdot \theta^2 + D^{(3)}_{ijkl} \cdot \theta^3)s_{kl} - e^{\theta}_{kij}E_k \tag{2.27}$$

Where C_{ijkl} is the same basic second-order elastic stiffness as previously defined, and $D^{(1)}_{ijkl}$, $D^{(2)}_{ijkl}$, and $D^{(3)}_{ijkl}$ are the first-, second-, and third-order total thermoelastic stiffnesses. Although their values are given directly, $D^{(1)}_{ijkl}$, $D^{(2)}_{ijkl}$, and $D^{(3)}_{ijkl}$ have the following theoretical definition, where $\tilde{C}^{(2)}_{ijkl}$ and $\tilde{C}^{(3)}_{ijkl}$ are the same 'effective' temper-

ature derivatives previously described:

$$D_{ijkl}^{(1)} = C_{ijkl}^{(1)} + C_{ijklmn}\alpha_{mn}^{(1)} \tag{2.28}$$

$$D_{ijkl}^{(2)} = \tfrac{1}{2}\tilde{C}_{ijkl}^{(2)} + C_{ijklmn}\alpha_{mn}^{(2)} \tag{2.29}$$

$$D_{ijkl}^{(3)} = \tfrac{1}{6}\tilde{C}_{ijkl}^{(3)} + C_{ijklmn}\alpha_{mn}^{(3)} \tag{2.30}$$

In the current work, the total thermoelastic stiffness method put forward by Yong and Wei was used sparingly overall. It was necessary for benchmarking the stress-free temperature-frequency response of known cuts and for very small pressures where convergence issues were encountered. But because the primary focus of this work was to achieve accurate frequency response versus changes in temperature *and pressure*, Lee and Yong's effective temperature derivative method was used elsewhere throughout. The Lee-Yong relations are fully capable of accurately modeling the stress-free temperature response of frequency, in addition to the combined stress-temperature or pressure-temperature response.

The correlation between the two methods will depend on the ratio of elastic strain to thermal strain; if it is small, then the 'thermal strain only' assumption of the total thermoelastic stiffnesses is accurate, and the small portion of third-order stiffness effects caused by stress-induced elastic strain can be neglected. Generally, this is the case, and examples of the close correlation between the two methods can be seen in the benchmark tests that involve both the Nonlinear and Linear Stressed Homogeneous Temperature Algorithms in the same study, the latter of which uses Yong and Wei's total stiffness terms, while the former uses the Lee and Yong method and values. These benchmarks can be found in Section 3.5.

CHAPTER 3

FINITE ELEMENT METHODOLOGY

3.1 Overview of the Finite Element Method

The finite element method, or FEM, is a diverse numerical computation tool whereby a complex physical problem is broken down into simpler more basic parts, or finite elements. For each element, an arbitrary function (usually a polynomial function of space) is assumed to describe the dependent variables to be solved, such as displacement or voltage. This function is called the *basis function* or *trial function*. Unknown coefficients that appear in the basis function, called degrees of freedom, are mapped to actual values of the dependent variables at specific points, or nodes, on each element. Theses mappings are known as shape functions. Shape functions allow the degrees of freedom to be coupled with information about how each element is physically connected to its neighbors, or in other words, how the original problem was broken down. This is the finite element skeleton; the bookkeeping that allows a reactive continuum to be described as a finite number of interconnected nodes, known as a mesh.

The 'complex physical problem' that is desired to be solved is usually in the form of a partial differential equation, or PDE. Such differential equations include thermoelastic equations of motion (or equilibrium), fluid dynamics laws like Navier-Stokes equations, or Maxwell's electromagnetic equations, among many others. In reality, the solution to the problem will be a spatial functional arrangement or field of the dependent variable that obeys the governing PDE at *every point* in the continuum. But within the finite element method, there is no continuum, per se, except that which

is interpolated from the nodal solutions after the fact. As previously described, the continuum is replaced with a network of points. Indeed the points represent the continuum in their vicinity, but their control over that continuum is limited by a combination of the degree of the assumed polynomial basis function together with the finite size of the elements themselves. In other words, the vector space of the solution is limited, when compared to that of the realistic continuum.

Therefore, applying the governing PDE to the finite element formulation must necessarily yield an approximate solution: the limited nodal function does not have to solve the PDE at *every* point if, on the whole, it is the *best representation possible* of the real function that does. The next logical question is, how does one know if the nodal solution is the best possible? After all, it will not likely be a solution to the actual differential equation. How can one tell if a wrong solution is "close enough?" The two most common answers to this question are by a) minimization of potential energy (or the Rayleigh-Ritz method) and b) Galerkin's method of weighted residuals. While the former is the simplest (one needs only to derive potential energy as a function of the degrees of freedom and then find the minimum using elementary calculus) the latter is the most general and also easier to apply when tens of thousands of degrees of freedom are involved. Galerkin's method converts the original PDE to an appropriate *weak formulation* that allows integration of the weighted residual, or error of the approximate function, over the entire domain. Knowing this quantitative value for the "overall error" of the approximate function, the best solution for the unknown degrees of freedom is defined as the one that that minimizes the total residual.

In the case of Galerkin's method, the error is "weighted" by a function that represents every kinematically feasible possibility for the solution (that is, every possibility that obeys the known displacement boundary conditions) with the same form as the basis or trial function (and thus in the same limited vector space). For Galerkin's method in solid mechanics problems, these weights are analogous to concept of virtual

displacements. Because the error in the approximate solution is weighted by virtual displacements that have the same limitations as the basis functions themselves, the *weighted* error of the correct solution integrated over the domain will be zero. This is paramount, because knowing the solution will yield an integrated weighted residual that is actually zero (rather than an arbitrary 'smallest number possible') transforms an elementary calculus problem of minimization into a linear algebra problem of solving an equality.

To better illustrate the operations involved in applying Galerkin's method, consider the following one dimensional example [19]. If the governing differential equation is of the form of a partial differential operator, L, operating on some function of space, $u(x)$, to yield some constant P:

$$L \cdot u(x) = P \tag{3.1}$$

Then the residual, $\varepsilon(x)$, is defined as the error of using an approximate trial function, $\tilde{u}(x)$, for the actual solution $u(x)$:

$$\varepsilon(x) = L \cdot \tilde{u}(x) - P \tag{3.2}$$

Thus, according to Galerkin's method, the integral of the weighted residual over the entire volume must equal zero:

$$\int_V \phi(x) \cdot \varepsilon(x)\,\mathrm{d}x = \int_V \phi(x) \cdot (L \cdot \tilde{u}(x) - P)\,\mathrm{d}x = 0 \tag{3.3}$$

Here, the weighting function is supplied as $\phi(x)$, where $\phi(x)$ and $\tilde{u}(x)$ are derived from the same basis functions. One simplistic example of the form of these functions would be:

$$\tilde{u}(x) = u_1 + u_2 x + u_3 x^2 \tag{3.4}$$

$$\phi(x) = \phi_1 + \phi_2 x + \phi_3 x^2 \tag{3.5}$$

Here u_1, u_2, and u_3 can be thought of as the degrees of freedom (although the shape functions as well as the positions and orientations of elements complicate this otherwise direct relationship) and the values of ϕ_1, ϕ_2, and ϕ_3 are arbitrary in that Equation (3.3) must hold for any and all values of these coefficients. Usually, integration by parts (or divergence theorem in multiple dimensions) is then applied to Equation (3.3) to reduce the order of the derivative operator and specify natural boundary conditions to the problem. The result is sometimes referred to as the *weak form* or *variational form*, which for static linear elastic problems happens to be equivalent to the *principle of virtual work* viewed in context of the the entire domain.

Within the finite element program, the integration over the domain can be performed programmatically, using Gaussian quadrature for example. Then knowing that the equality to zero in Equation (3.3) must hold for any value of virtual displacement (ϕ_1, ϕ_2, ϕ_3, $\ldots$,ϕ_n) each additive term containing ϕ_n must also independently be equal to zero. It so happens that all additive terms do contain exactly one ϕ_n, where the highest n is also the total number of degrees of freedom. So grouping the equality by like terms of ϕ_n yields exactly as many equations as there are unknown degrees of freedom, and in this way, the entire process is reduced to the solution of a system of linear equations in matrix form.

The above example of applying Galerkin's method is just one of the many methods of weighted residuals, and is a good simplified representation of finite element method involved in the current work. By contrast, some modern finite element codes are found to employ a completely different fundamental arrangement, such as mesh-free methods. For more information about the details of the finite element method, many textbooks are available including *Introduction to Finite Elements in Engineering* by Chandrupatla and Belegundu [19].

3.2 Finite Element Method in the Current Work

When the finite element method is applied in engineering analyses, it usually involves commercial software designed for that purpose. As such, the governing equation is selected by default by the type of model ran, and the user needs only provide the inputs such as the meshed geometry and boundary conditions. However, looking at the governing equations for the current work derived in Equations (2.13) and (2.10) (that is the modified elastic equation of motion and Gauss's Law for an insulator) together with the definitions in Equations (2.15) and (2.16) and beyond, one can see that the governing equations for the incremental model, which mix in the results from the initial model, are not likely to be the default of any commercially available program. Indeed, the software used in this project, COMSOL Multiphysics, was chosen specifically because the default definitions for variables and the governing weak form equation are visible to the user and also easily revised. Furthermore, those default definitions already include many simulations that involve multiple physical laws, such as the coupled mechanical and electrical response present in a piezoelectric material. COMSOL Multiphysics versions 3.5a and 4.1 contributed to separate parts of the results attained in this study, although 4.1 was primarily used.

The *initial* model and the *incremental* model, previously described in Section 2.4, were assembled in the COMSOL environment to run sequentially. Deriving the weak form expression from the partial differential equation in Equation (2.13) for input into COMSOL was completed and verified against a similar derivation for COMSOL's default weak form. In fact, this default governing equation was found to be a special case of the incremental governing equation (2.13) where initial model response is zero for initial displacement, initial strain, and initial stress ($U_i = 0$, $S_{ij} = 0$, and $T_{ij} = 0$ from the previous chapter). Both the initial and incremental models incorporated the material definition given in Section 2.5 by means of a custom material library within COMSOL. This material library held functions that took the needed inputs for

temperature and strain directly from the model in order to output accurate material properties throughout the domain of the resonator (the strain input yielding the nonlinear third-order elastic effects).

The other fundamental modification to the default COMSOL Multiphysics interface was the addition of global variables to link the results of the initial model to the inputs of the incremental model at every point in the domain. This provides a one-way bridge of information to solve the initial and incremental models in sequence. Looking through the incremental equations previously provided in Equations (2.11) through (2.16), one can see the references to the initial model include three basic sets of data: the initial displacement derivatives $U_{i,j}$, the initial strain S_{ij}, and the initial stress T_{ij}. The global linking variables were derived directly from these three sets.

Besides these modifications, there were other general considerations that are necessary for any finite element model. Because all of the resonator cuts studied in the current work operate on the thickness-shear mode of vibration, the mesh density in the thickness direction was a primary consideration for convergence of the solved frequency response. A swept mesh format allowed precise control the number of mesh layers in the thickness direction. A simple convergence study of a round AT-Cut quartz resonator with a nominal fundamental mode frequency just under 10 MHz, shown in Figure 3.1, found that the solved frequency value changed very little above a mesh density of ten mesh layers per half wavelength. That is, at the fundamental thickness shear mode, ten mesh layers were sufficient to model the entire thickness of the resonator. At the third overtone, the domain contains one-and-a-half lengths of the resonant standing wave at any given time, so 30 mesh layers are recommended.

Another general consideration for most finite element models is the application of symmetry. It is important to note in the current work that while the boundary conditions and geometry often allowed two-fold, four-fold, or even eight-fold symmetry, the anisotropic material properties of quartz do not generally comply with the same

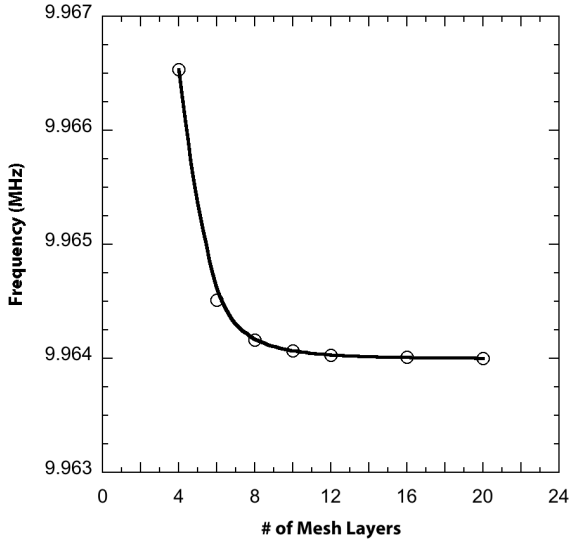

Figure 3.1: Mesh convergence: solved frequency vs. number of mesh layers

symmetry planes, and therefore disallow these simplifications. Likewise, most quartz simulations should require modeling the entire resonator geometry for an accurate frequency response because of quartz's anisotropy.

Finally, while the governing equations of motion previously discussed would allow the model to be based on the transient time-dependent behavior of the crystal, a more computationally-efficient solution for the resonate frequency is based on solving for the eigenvalues, or eigenfrequencies, of the model. Such a solution is independent of the time domain, because it solves the model for specific sets of displacement fields (the eigenfunctions or eigenmodes) which are assumed to be of harmonic form. The result is a list of eigenfrequencies of the model near a provided target frequency, together with their corresponding eigenmodes. By investigating the eigenmodes individually, one can identify which has the displacements corresponding to thickness-shear resonance, and thereby identify the resonant frequency. Because the piezoelectric effects are confined to the incremental model, the eigenvalue solution method is only relevant to solving this model and not the initial model.

3.3 Stressed Homogeneous Temperature Algorithms

The schematic flow for implementation of the finite element method as developed for the current work follows directly from the material considerations in Sections 2.4 and 2.5 and the methodology described in the previous Sections 3.1 and 3.2. For the most general algorithm used in this study, the entire domain of the resonator was assumed to be at a single homogeneous temperature. Any external pressure loading, geometric and elastic nonlinearity, and steady uniform change in temperature from the reference temperature was taken into account for the initial model. The nonlinear aspects of the initial model dictated that an iterative method be used until convergence was achieved. This iteration was performed by default within the software. Then the results of the initial model in terms of initial displacement gradient, initial strain, and initial stress ($U_{i,j}$, S_{ij}, and T_{ij} as previously described) were fed into the incremental model, which used the incremental piezoelectric governing equations together with the eigenfrequency solver to output the resonant frequency of the quartz oscillator. This process for the Nonlinear Stressed Homogeneous Temperature (NSHT) Algorithm is laid out in Figure 3.2. It should be noted that this algorithm is general enough so as to handle both the stressed and stress-free cases equally well, whereas the Stress-Free Homogeneous Temperature Algorithm described in the next section makes the literal assumption that initial stresses are zero, and thus is restricted to that scenario.

With additional governing equations (such as Fourier's Law of conduction) and appropriate material definitions (such as thermal capacity and anisotropic thermal conductivity) which were not previously discussed, the Nonlinear Stressed Homogeneous Temperature Algorithm could easily be adapted to model complex heterogeneous temperature fields and even transient thermal frequency response. Such models are not of interest in the current study, however, but can be referenced in work by Patel [14].

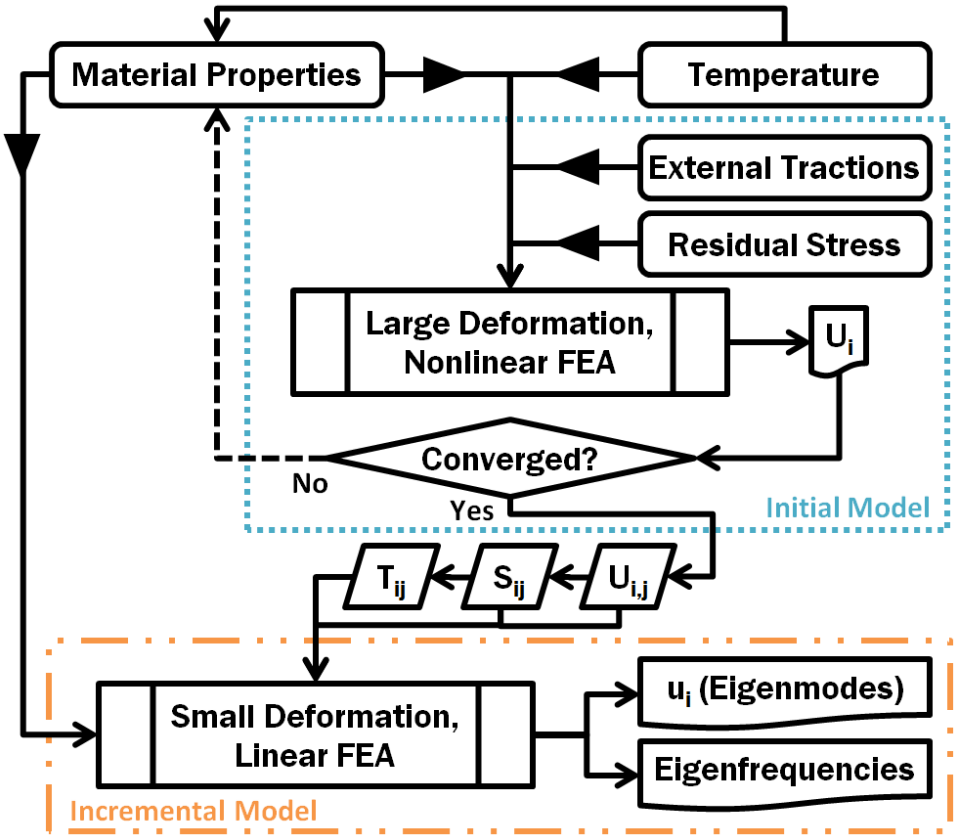

Figure 3.2: Flowchart for the Nonlinear Stressed Homogeneous Temperature Algorithm

Based on this algorithm, a similar algorithm was developed with the additional assumption that the initial response could be modeled linearly in a finite element sense. This assumption became necessary due to convergence issues within the nonlinear initial model when zero or otherwise relatively small external pressure loads were applied. As a side effect, the Linear Stressed Homogeneous Algorithm had the additional advantage of being much faster to run, because iteration was not necessary on the initial model. The initial model was linear in a finite element sense because the inputs (material properties) did not depend on the outputs, or the dependent variables (displacement and strain) of the model. The material properties were still modeled as analytic nonlinear functions of temperature, however, with homogeneous thermal strains implicitly assumed as inputs for the nonlinear third-order elastic response, using the 'total thermoelastic stiffness' data discussed in Section 2.5. This made the linear model a good approximation for the low-pressure scenarios it was designed to cover, because in these cases most of the strains are in fact due to thermal expansion and not the elastic response to external forces. Still, the nonlinear algorithm was used in favor of the linear algorithm in the current study wherever permissible by convergence, with the expectation it would be more accurate, especially at higher pressures. The Linear Stressed Homogeneous Temperature (LSHT) Algorithm is demonstrated in Figure 3.3.

3.4 Stress-Free Homogeneous Temperature Algorithm

As the ultimate simplification of the previously described algorithms, the initial finite element model can be completely eliminated and replaced by nonlinear analytic expressions to provide the incremental model inputs of initial displacement gradient, initial strain, and initial stress ($U_{i,j}$, S_{ij}, and T_{ij}, respectively). Because of the stress-free assumption, all initial strains and displacements must come from homogeneous thermal expansion, α^{θ}_{ij}, alone. In equation form, the stress-free assumption can be

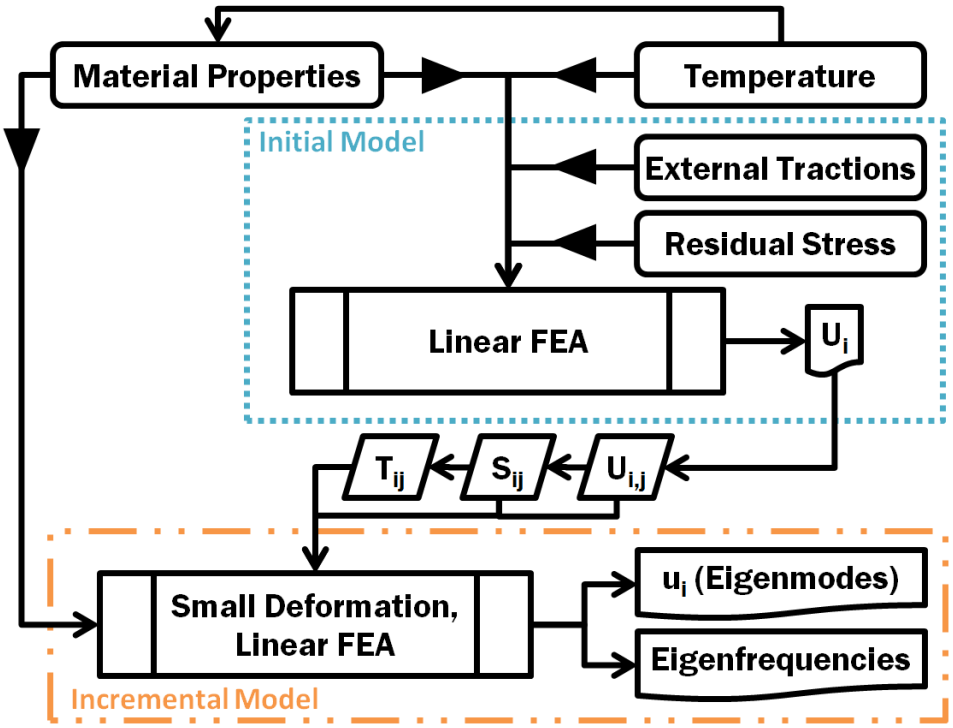

Figure 3.3: Flowchart for the Linear Stressed Homogeneous Temperature Algorithm

written as:

$$\alpha_{ij}^{\theta} = \alpha_{ij}^{(1)} \cdot \theta + \alpha_{ij}^{(2)} \cdot \theta^2 + \alpha_{ij}^{(3)} \cdot \theta^3 \qquad ((2.20))$$

$$U_{j,i} = U_{i,j} = S_{ij} = \alpha_{ij}^{\theta} \qquad (3.6)$$

$$T_{ij} = 0 \qquad (3.7)$$

Note that the quadratic finite strain terms for the initial strain S_{ij} (that is, $\frac{1}{2}\alpha_{ki}^{\theta}\alpha_{kj}^{\theta}$) were dropped because they are on the order of 10^{-3} smaller than the linear term α_{ij}^{θ} and therefore negligible [12]. The stress-free assumption was exactly the condition for which the 'total thermoelastic stiffness' material data was derived by Yong and Wei [11] as discussed in Section 2.5, so this data was used to calculate the linear stiffness for the incremental model as given in Equation (2.26). Thus, the Stress-Free Homogeneous Temperature (SFHT) Algorithm is illustrated in Figure 3.4. Note that this stress-free algorithm is also linear in a finite element sense.

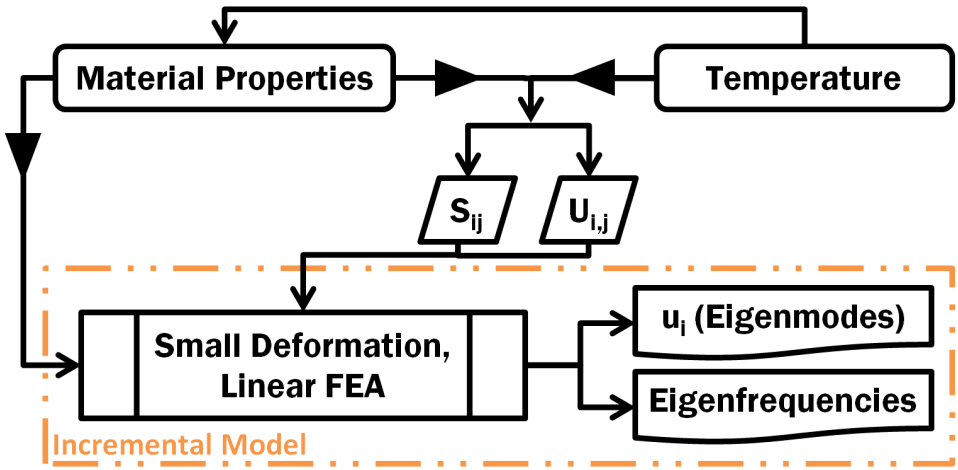

Figure 3.4: Flowchart for the Stress-Free Homogeneous Temperature Algorithm

3.5 Model Benchmarks

After the previously-described algorithms were developed, they were compared against experimental data from literature for benchmarking purposes, beginning with the simplest Stress-Free Homogeneous Temperature Algorithm. The incremental model in this algorithm was used on a rectangular AT-Cut ($(YXl)35.25\,°$) plate geometry with dimensions the same as that studied in Chapter 7 of Mihir S. Patel's dissertation [14], henceforth referred to a simply Patel's dissertation. Following his geometry, the resonator is composed of a 1.7 millimeter by 1.2 millimeter by (approximately) 30 micron thick rectangular quartz domain, and also includes the modeling of two thin (0.1 micron thickness) gold electrodes as an isotropic linear elastic material in the finite element model. The primary contribution of this layer to the frequency results of the model was found to be the added mass contribution that lead to a decrease in the resonate frequency, as would be expected. Also some spurious modes of vibration in the resonator seemed to be dampened out somewhat by modeling the gold, but this could have been an indirect consequence of the downward shift of the frequency of the resonate mode away from the ailing spurious modes. After the stress-free algorithm, the Linear Stressed Homogeneous Temperature Algorithm was then also applied to

Patel's geometry. The details of the geometric dimensions can be found in Chapter 7 of Patel's dissertation. The meshed geometry, an example solution from the current study, and the results for both algorithms as compared to Patel's data are given in Figure 3.5, recalling that LSHT and SFHT stand for 'Linear Stressed Homogeneous Temperature' and 'Stress-Free Homogeneous Temperature' Algorithms, respectively.

To highlight the change in frequency as a function of temperature and to further normalize for geometric dissimilarity, it is customary to report frequency data as a change in parts per million from the frequency at a reference temperature, usually 25 °C (with no pressure or force load applied, if applicable). The same approach was taken here, with the frequency change being calculated as $(f - f_0)/f_0$ where f is the measured frequency and f_0 is the frequency at the reference temperature. Thus the trends themselves become all the more relevant compared to small offsets in frequency that vary from resonator to resonator (or simulation to simulation) that get eliminated from the study. This analysis technique finds advantage in the remarkable sensitivity of quartz resonators, and in reporting of the properties of the numerous cut angles. In fact, the removal of a single layer of silicon atoms from a 1MHz X-Cut quartz plate 3mm thick would increase the frequency by about 0.1 Hz [1]. So absolute repeatability of frequency magnitude is not easily achieved, but the frequency response *trends* visible in a given cut are much more duplicable.

In Patel's work, a near-identical model and algorithm is developed for a much different ultimate goal of examining glass-packaged quartz resonators. Such an assessment was of great value because it not only allowed comparison to experimental data compiled by Patel from previous studies, but also comparison to the data from Patel's finite element models themselves. As seen in Figure 3.5, the algorithms of the current study agree quite well with Patel's data, often falling between Patel's own "FEM Static f-T Model" and the actual experimental data. The small deviation

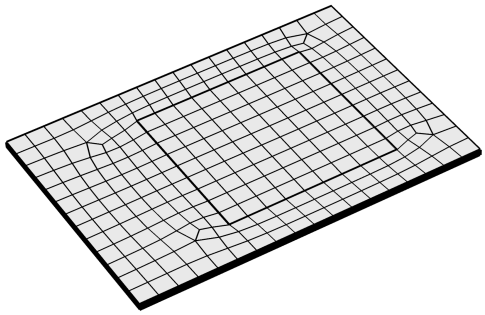

(a) Meshed geometry

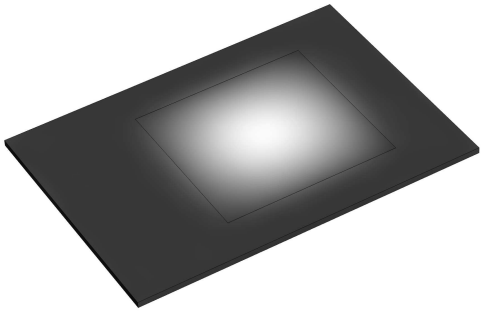

(b) Example eigenmode displacement

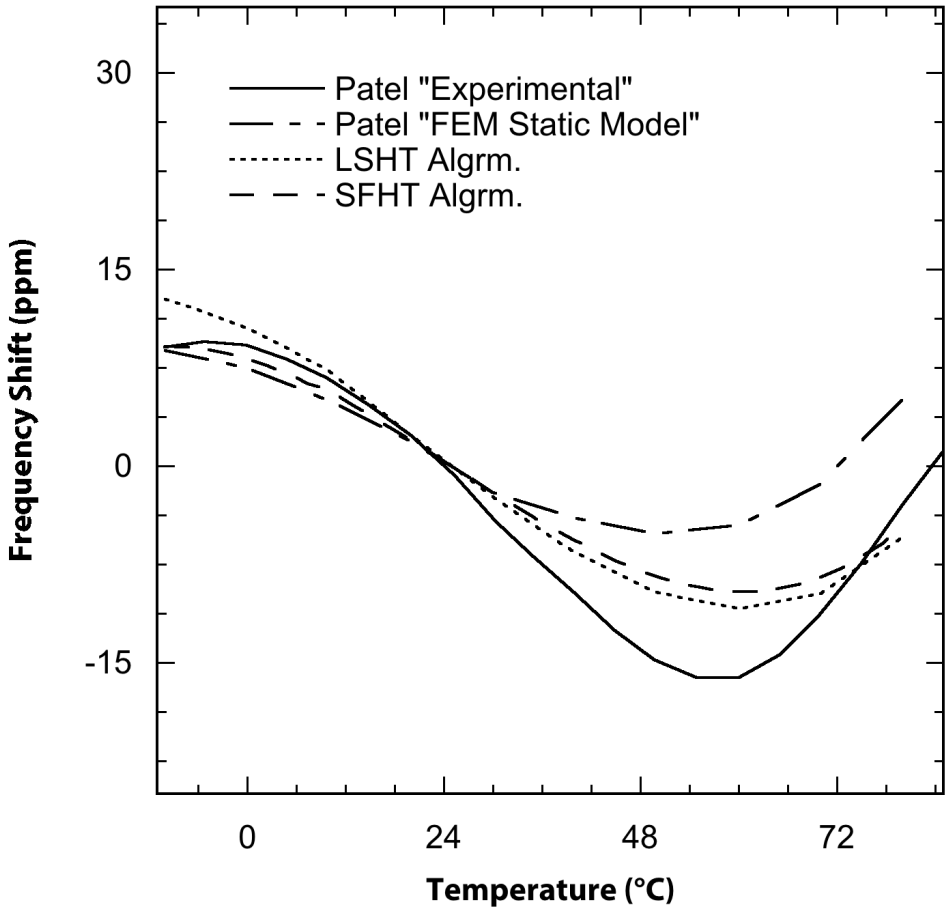

(c) Frequency shift vs. temperature

Figure 3.5: Benchmark data: stress free AT-Cut (reference data from Patel [14])

from experimental values could be accounted for by uncertainty in the experimental resonator's cut angle, which for the AT-Cut directly affects the amount of turnover (or difference between the characteristic relative minimum and relative maximum) which is present in the response. The even smaller difference between the Stress-Free Homogeneous Temperature Algorithm and the Linear Stressed Homogeneous Temperature Algorithm themselves is likely due to the fact that the thermal strains are analytically fed into the incremental model during the stress-free algorithm, while they are approximated by the solution of the initial model in the stressed algorithm. Patel shows a similar discrepancy between his "dynamic" and "static" models [14].

Using the same geometry, Patel also demonstrates his model's prediction for the stressed frequency response of the crystal by using fixed boundary conditions all along the edge of the rectangular resonator. The resultant plot, although not entirely exciting, does provide an additional point of reference for the stressed algorithms. Note that the stress-free algorithm would fail conclusively, since its assumption of free-expanding thermal strains would be entirely wrong. In fact, the stress-free algorithm would show little to no reaction to this change in boundary conditions on the far edges of the plate (this is confirmed explicitly by Patel [14]). Besides the fixed edges, all other aspects of the target geometry remained the same. Patel's results are given with comparison to the Linear Stressed Homogeneous Temperature Algorithm in Figure 3.6.

Except for the small dip in the Patel model's response at 35 °C, both plots are linear and match up very well. The dip could be the result of the interference from a spurious mode, which has the effect of knocking the resonate frequency off of its indented value. The causes of spurious or inharmonic modes are discussed at length by Bottom [2]. Basically they are caused when the primary mode of vibration (i.e. thickness-shear) is tainted by the resonance of an otherwise irrelevant mode (for instance, an extensional mode overtone) at a nearby frequency. Often the spurious

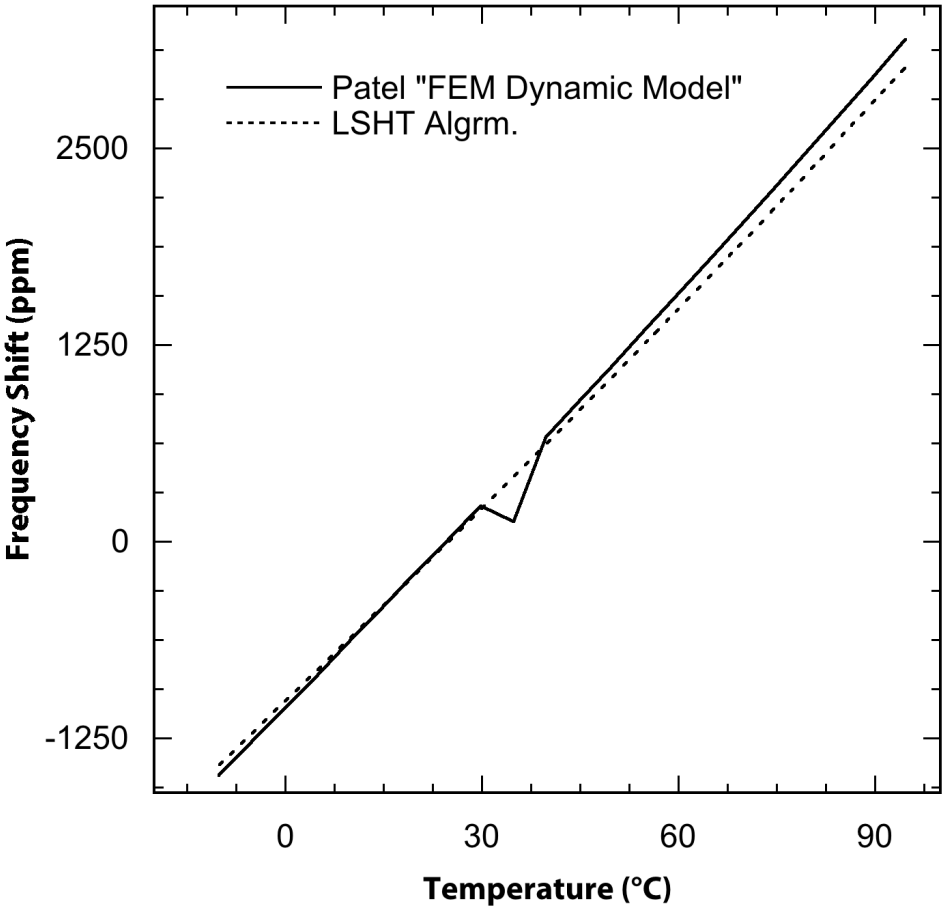

Figure 3.6: Benchmark data: fixed edge stressed AT-Cut (reference data from Patel [14])

modes have totally different responses to external factors, such as temperature change, and so the spurious response of the primary mode is intermittent, whenever such an irrelevant mode happens to the in primary mode's vicinity of the frequency spectrum. The effects in reality include increased resistance (and decreased response, known as an 'activity dip') of the resonator and a lower quality factor, among others. The effect in the incremental model is a slight pull of the resonant frequency away from its otherwise predicted value. The reason that the spurious mode is not present in both models could be that, in the FEM environment, the exact frequency location of a spurious mode can be highly dependent on the mesh shape and density, since it is not often a well-defined mode of vibration according to the dominate physics of the problem. In any case, the dip at 35 °C is definitely no trend and this benchmark is satisfactorily passed by any account.

To continue benchmarking the algorithms developed for this study, focus was turned to work done by Errol P. EerNisse. First his article from 1975 [20], involving what he referred to as the "stress coefficient" of frequency, denoted by K. In this work, EerNisse performs calculations that show the frequency shift with respect to in-plane biaxial stresses to be linear and proportional to the stress, or pressure, applied (much like the result to the previous benchmark). Therefore, unlike the complex temperature response, the pressure response of frequency can be quantified by a single number representing the slope of the linear plot. This slope determines the value of EerNisse's stress coefficient, and is different for different cuts of quartz. EerNisse's calculated values for the AT-, BT-, and SC-Cuts are compared to the output from the Nonlinear Stressed Homogeneous Temperature Algorithm. The cut angles used in the algorithm are denoted by $(YXl)35.25\,^\circ$, $(YXl)-49.00\,^\circ$, and $(YXwl)22.4\,^\circ/33.88\,^\circ$ according to the *IEEE Std 176-1949* convention for the AT-, BT-, and SC-Cuts, respectively. EerNisse does not describe in detail the geometry assumed in his calculations. The geometry was assumed to be a common form: round, plano-plano (meaning flat on both sides

rather than curved like a lens) resonator with central round electrodes (not modeled with a gold layer, but only as the electrical boundary condition). The temperature was assumed to be 25 °C. The biaxial stress was applied using a compressive pressure traction applied evenly across the entire outer edge of the fattened cylindrical shape. This would correspond to EerNisse's "stress anisotropy" ratio of one. Figure 3.5 shows the meshed resonator geometry, and Table 3.5 shows the excellent numerical agreement between the Nonlinear Stressed Homogeneous Temperature Algorithm and EerNisse's calculations. Note the near-zero value of K for the 'stress compensated' or SC-Cut, which EerNisse himself developed specifically for this attribute.

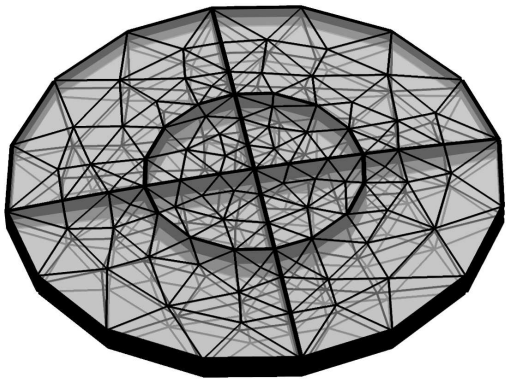

Figure 3.7: Resonator geometry mesh for stress coefficient benchmark

Quartz Cut	Stress Coefficient, K ($10^{-12}\,\mathrm{cm}^2\,\mathrm{dyne}^{-1}$)	
	Current Work	EerNisse (1975) [20]
AT	2.773	2.75
BT	–2.626	–2.6
SC	0.004	0.0

Table 3.1: Benchmark data: stress coefficient of frequency

A later experimental analysis by EerNisse [21] from 1980, which also included data from C.R. Dauwalter [22], served as a final benchmark for the stressed algorithms. This study examined the temperature dependence of the "force frequency coefficient"

with symbol K_f, which has a similar definition as the stress coefficient previously discussed, except rather than a biaxial stress state, the force coefficient describes the linear frequency response to diametrically-opposed point-load compression forces on a circular resonator. The equation defining the use of the force coefficient is given by [21]:

$$\frac{f - f_0}{f_0} = K_f \frac{F \cdot N_0}{d \cdot \tau} \tag{3.8}$$

The left side of Equation (3.8) is easily identified as the fractional frequency shift discussed previously, F is the magnitude of the applied diametric force in newtons, and N_0, d, and τ are all constant for a given resonator (and are the frequency constant in meters per second, resonator diameter in meters, and resonator thickness in meters, respectively). This allows K_f to define the slope of the linear frequency response as F is increased (with units of $\mathrm{m \cdot s \cdot N^{-1}}$). Another parameter which is of importance in this study is the azimuthal angle ψ that defines the location on the perimeter where F is applied, measured in degrees counterclockwise around the rotated +y-axis (y''), which is normal to the plate, from the rotated +x-axis (x''). Since the loading is applied on opposite sides of the resonator, ψ needs only range from zero degrees to 180 degrees in order to demonstrate every value of K_f for a given cut. While EerNisse gives experimental data for the AT-, FC-, SC-, and X-Cuts, the current benchmark was limited in scope to the AT-Cut, which Dauwalter had previously explored in 1972 [22]. Thus, the experimental value of K_f as a function of the diametric angle of the applied load, ψ, for the AT-Cut was compared to the same prediction by both the Nonlinear Stressed Homogeneous Temperature Algorithm and the Linear Stressed Homogeneous Temperature Algorithm of the current study. First looking at only the response at the reference temperature of 25 °C, the results are plotted in Figure 3.8. In this figure, one can see that both the linear and nonlinear algorithms match the experimental values very closely. Incidentally in the algorithms' predictions, K_f is assumed to be symmetric about $\psi = 90°$, just as in the experimental data [22], so that

more data points could be taken in the time and memory allotted for the simulation.

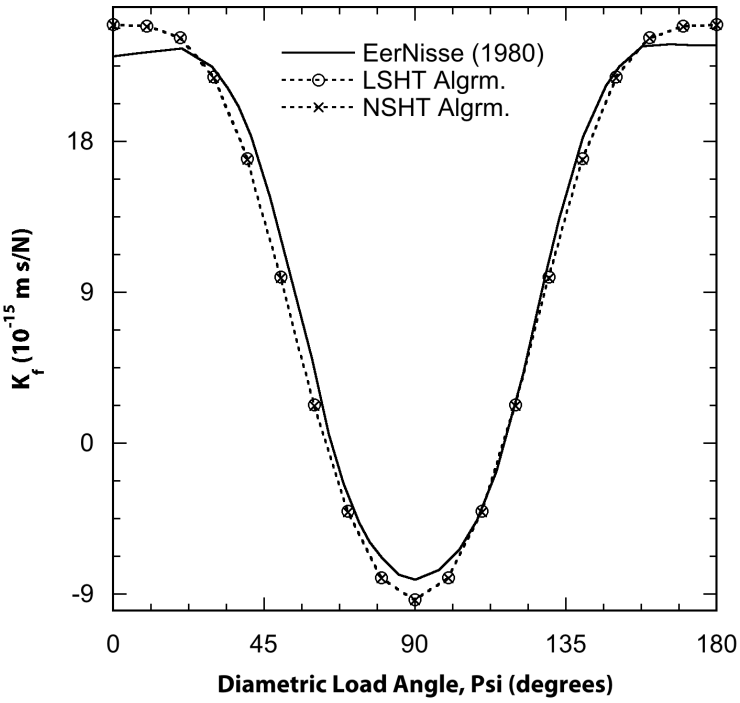

Figure 3.8: Benchmark data: force frequency coefficient, K_f, for the AT-Cut (reference data from Dauwalter [22] and EerNisse [21])

Both EerNisse and Dauwalter also provide the change in force frequency coefficient, K_f, with respect to change in temperature, T, as a first order derivative, $\mathrm{d}K_f/\mathrm{d}T$ (with units $\mathrm{m} \cdot \mathrm{s} \cdot \mathrm{N}^{-1} \cdot {}^{\circ}\,\mathrm{C}^{-1}$), and it is here that the algorithms for the current study, which had performed very well in benchmarks up to this point, begin to show their weakness. As seen in Figure 3.9, the Dauwalter data (which EerNisse data confirms, although it is not repeated here) shows a definite trend in this temperature derivative $\mathrm{d}K_f/\mathrm{d}T$ as a function of diametric angle, ψ. Such desired response from the linear algorithm tested effectively flatlines, with negligible temperature-induced change in K_f for all angles ψ. Because K_f itself is directly proportional to the derivative of frequency with respect to change in pressure (it determines the slope of the frequency-pressure curve), then $\mathrm{d}K_f/\mathrm{d}T$ is proportional to the second-order mixed

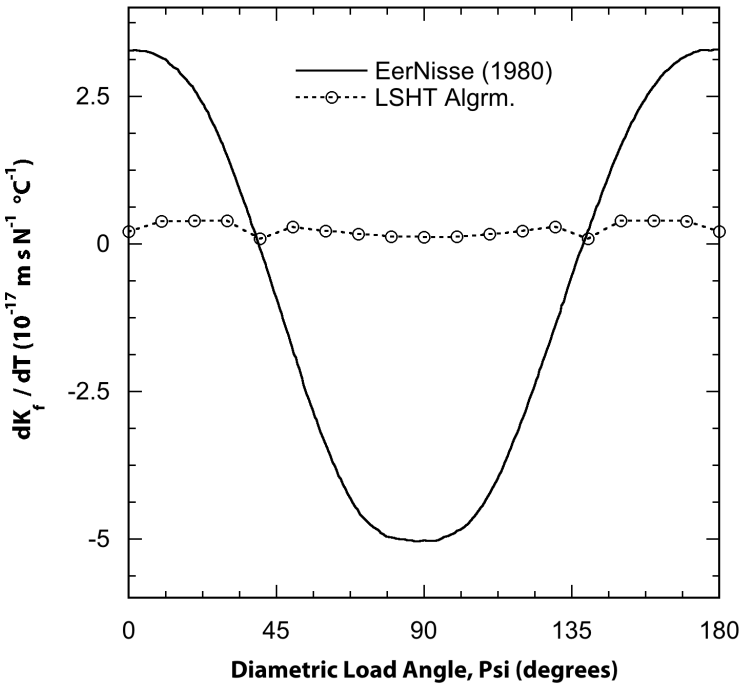

Figure 3.9: Benchmark data: first temperature derivative of K_f for the AT-Cut (reference data from Dauwalter [22] and EerNisse [21])

partial derivative of frequency, $\partial^2 f / \partial T \partial P$. That is:

$$K_f \propto \frac{\partial f}{\partial P} \tag{3.9}$$

$$\frac{dK_f}{dT} \propto \frac{\partial^2 f}{\partial T \partial P} \tag{3.10}$$

A hypothesis of the current work is that the inaccuracy of the current algorithms in predicting the second-order mixed temperature and pressure response characterized in Equation (3.10) (and also Figure 3.9) is due to the unavailability of certain constitutive material properties, being the temperature derivatives of the 3rd-order elastic stiffness as initially categorized in Table 2.1. Another vantage point for this issue is provided as a side-effect of modeling the frequency response of the quartz temperature and pressure sensor, which is the subject of the next chapter.

CHAPTER 4

FREQUENCY RESPONSE OF THE TEMPERATURE-PRESSURE SENSOR

4.1 Sensor Geometry

As mentioned in the first chapter, quartz resonators are well suited to serve as temperature and pressure sensors due to the unique physical properties of quartz. This is especially true for downhole applications in the oil and gas industry, which take full advantage of the compactness and long-term stability of the quartz resonator and also benefit from its fine resolution and accuracy.

The sensor geometry investigated in the current study is one in which a flat-sided cylindrical casing surrounds a circular resonator, as shown in Figure 4.1. This casing, formed by two sealed end caps, mechanically serves to actuate the state of hydrostatic pressure on the exterior as a non-uniform biaxial compressive stress across the interior resonator plate.

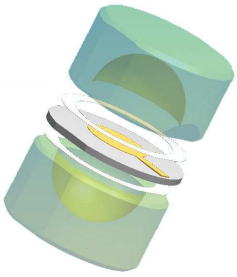

Figure 4.1: Quartz pressure sensor geometry with end caps [23]

Although nominally referred to as a "pressure" sensor, such a device does have a considerable temperature response and is thus technically a temperature-pressure sensor. Therefore to measure both, an independent temperature measurement must also be made. This is most simply accomplished with a standard clip-mounted resonator, which can be isolated from external pressure, and possibly cut at special angles that are well known to produce desirable temperature response for use as thermometers [24]. It is therefore significant that the simulation be able to output both the pressure and temperature response of the "pressure" sensor, as this allows the simulation to predict how easily the two responses can be separated for a given pressure sensor design.

4.2 Simulation Overview

Thus, the Nonlinear Stressed Homogeneous Temperature Algorithm laid out in Section 3.3 was employed on the previously described pressure sensor geometry. Experimental data was collected from two such sensors. While the initial model in the algorithm was necessarily used on the entire sensor geometry to model the effect of the end caps, the incremental model was limited to the resonator plate itself to save computational time and memory. Thus the incremental model pulls only those input values of initial displacement, initial strain, and initial stress that are spatially needed for its solution, although such values are available for the entire geometry.

Because of the size and complexity of the complete meshed geometry, limitations on available memory dictated that certain simplifications be made beyond what may have been considered ideal. The gold electrodes were not modeled in bulk, but simply the electrical boundary conditions they impose. While this has the effect of raising the predicted frequency by a few percent versus a model with the extra gold mass, it should have minimal effect on the pressure and temperature dependent *trends* in response. Similarly, the number of swept layers through the thickness of the resonator

was reduced to about seven per half-wavelength (see Section 3.2 for description). Again, while a slight reduction in the absolute accuracy of the frequency can be expected, the trends are much more dependent on the inputted boundary conditions and material properties. In this way, the quantity of degrees of freedom for the initial model was brought to 125709, with 160366 for the incremental model, the latter still more since it has the additional piezoelectric physical parameter of voltage to solve for at each node, in addition to the X-, Y-, and Z-direction displacement. Since the nominal size of the finite element stiffness matrix involved in calculation is proportional to the square of the degrees of freedom, these values were near the memory limits for the computer used in the analysis. The entire nonlinear simulation had a runtime of about 30 hours.

4.3 Results

The result of the simulation is frequency response as a function of two independent variables: applied temperature and external pressure. This data can be represented on the whole as a three-dimensional surface plot. Alternatively for closer inspection, slices of the response at constant pressures (isobaric) or constant temperatures (isothermal) can be viewed as a normal scatter plot. This will be the method used in the current work. Because the experimental data did not contain a data point at 25 °C and 0 psi for a standard reference, both the experimental and simulation values where normalized to the frequency at 50 °C and 14 psi (external pressure) for the calculation of frequency shift in parts per million. Also it should be noted that the experimental batches A and B contain a slightly different input set of temperature and pressure points, most notably that A contains data up to 20,000 psi and 200 °C while B only goes up to pressures of 16,000 psi and temperatures of 175 °C.

Taking the approach of using isothermal and isobaric slices of the surface plot as previously described, the output of the Nonlinear Stressed Homogeneous Temperature

Algorithm (abbreviated 'NSHT Algm.' in the plots) yields Figure 4.3 for the isobaric case and Figure 4.2 for the isothermal case. Correlation between the experimental data and the simulation is fairly good overall, which each major experimental trend being mirrored in the output of the algorithm. For the isothermal plots, the pressure response is linear, and the slope of the line in the simulation is near the experimental slope, especially at low temperatures. At higher temperatures however, the experimental slope of the pressure response decreases while the simulation's slope increases very slightly. This results in the simulation's small error compared to experimental values of 7.52% at 50 °C and 20,000 psi growing to 25.65% at 200 °C and 20,000 psi. The same progressive path of the endpoints of the isothermal lines growing apart (because of opposite changes in the slope of those lines) as temperature increases can be more easily seen in a single instance in the isobaric plot for 20,000 psi, Figure 4.3(f).

For the isobaric plots, temperature response at low pressures shows the concave-up half of the characteristic 3rd-order polynomial-like curve of the AT-Cut (above the inflection point which occurs around 20 °C to 30 °C). Note that the slope of the temperature response of frequency is approximately zero near room temperature, as is the cut's design intent. The exact angle of the AT-Cut's X-axis rotation near 35.25° is known to influence the degree of this concavity, so the slightly-shallower dip present in the experimental values could be a result of the experimental cut angle tolerance. In any case, however, it can be seen that the experimental temperature response flattens out quicker with increasing pressure, and even becomes slightly inverted, whereas the simulation does not flatten out as much and never becomes inverted.

4.4 Conclusions

It is these experimental trends of trends, like the flattening and inversion of the temperature response with increasing pressure or the decreasing slope of the pressure

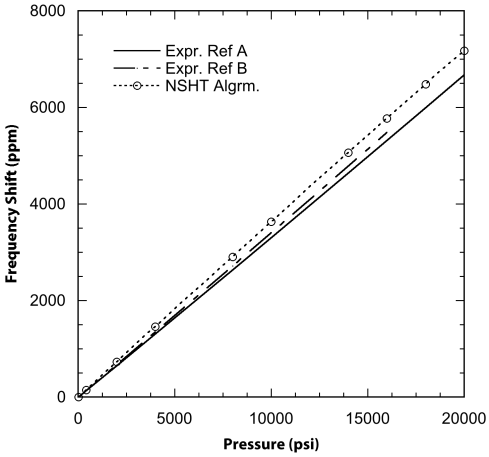

(a) T = 50 °C

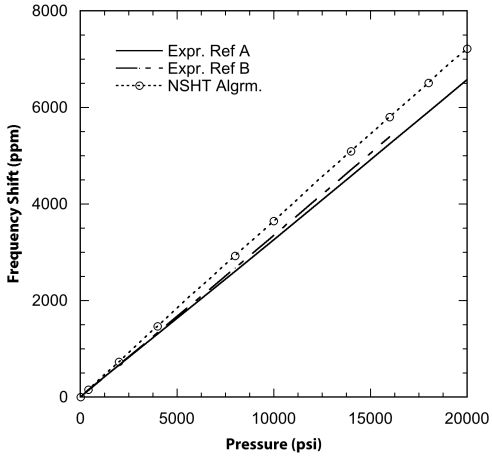

(b) T = 75 °C

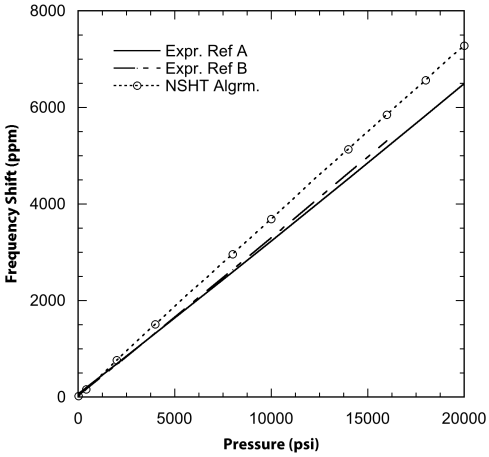

(c) T = 100 °C

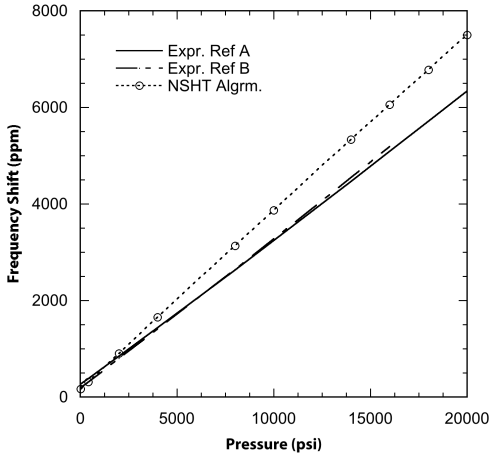

(d) T = 150 °C

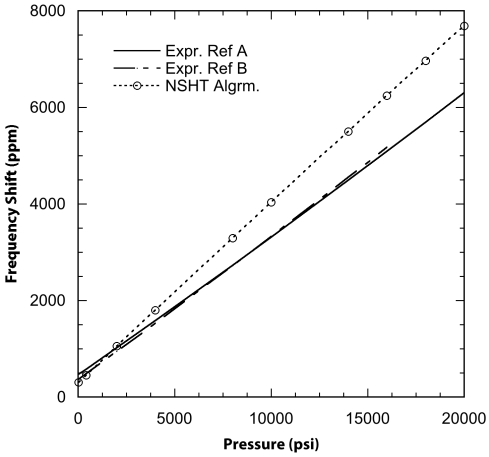

(e) T = 175 °C

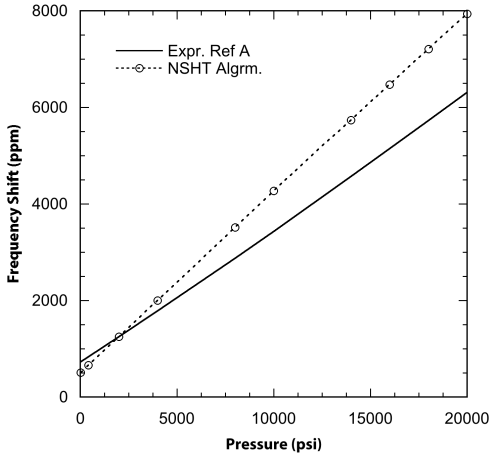

(f) T = 200 °C

Figure 4.2: Isothermal frequency-pressure sensor response

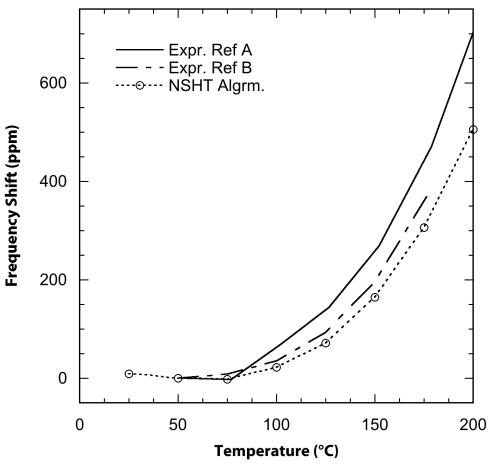

(a) P = 14 psi

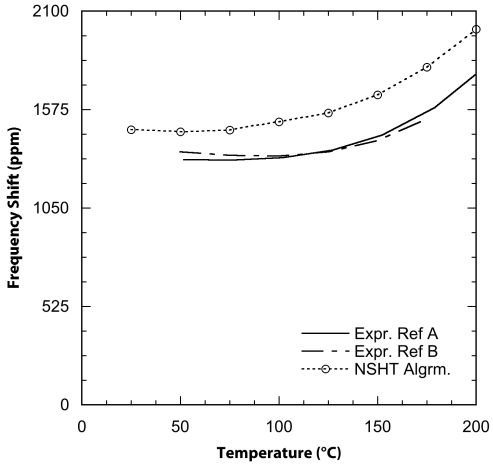

(b) P = 4,000 psi

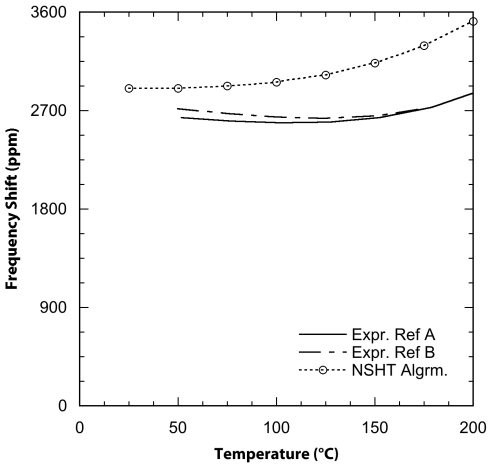

(c) P = 8,000 psi

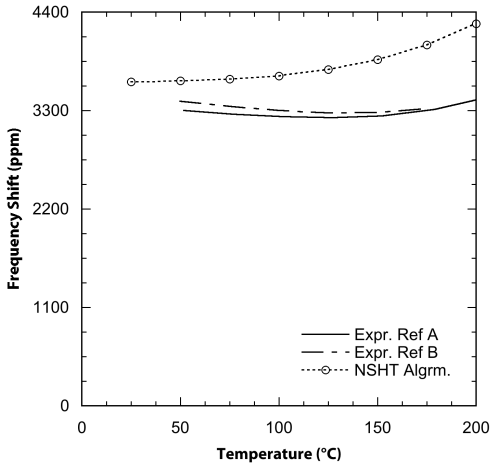

(d) P = 10,000 psi

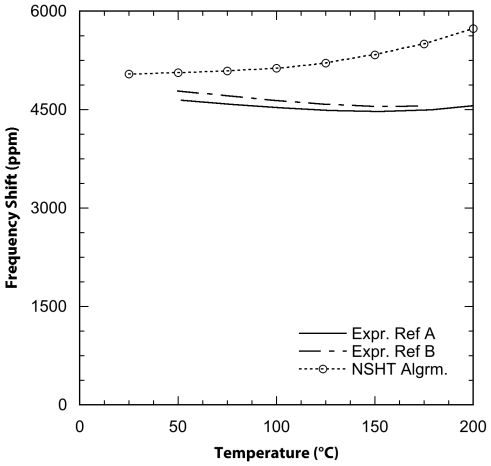

(e) P = 14,000 psi

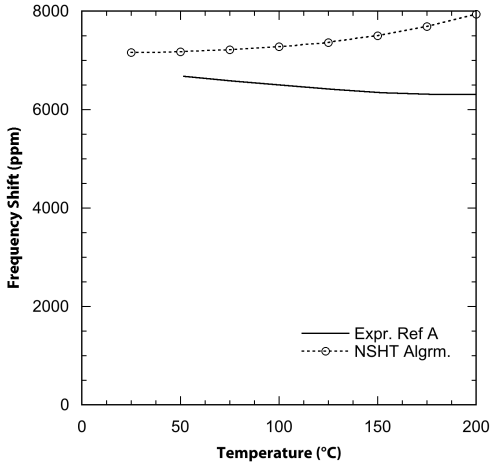

(f) P = 20,000 psi

Figure 4.3: Isobaric frequency-temperature sensor response

response with increasing temperature, that represent the effect of second-order mixed derivatives of frequency response with respect to temperature and pressure (as previously discussed at the end of Section 3.5). These mixed second-order effects can be attributed to the temperature derivatives of the 3rd-order elastic stiffness coefficients, for which numerical values are not currently available in literature, and thus also not present in the finite element simulation. The short answer behind why this link exists is given indirectly by EerNisse and Wiggins [24] who attribute the third-order elastic stiffness coefficients as the gateway to the frequency shifts due to a stress bias. In other words, they acknowledge that the nonlinear elastic terms control the pressure response of frequency. Therefore, in order for the pressure response to change accurately with temperature, the 3rd-order elastic coefficients also need to change accurately with temperature in the material definition. The accurate change of the 3rd-order elastic coefficients with temperature is, of course, given by their temperature derivatives as described in Equation (2.18).

For additional logical evidence to pin the blame on the temperature derivatives of the 3rd-order elastic stiffness, first consider the simplified one-dimensional equation for the nominal speed of a wave though a solid medium without dispersion, given in Equation (4.1). Note that, for quartz, such a velocity would directly affect the frequency of resonance.

$$v = \sqrt{\frac{c}{\rho}} \tag{4.1}$$

Here, v is the nominal velocity in, for instance, meters per second. Then c is the stiffness of the medium in newtons per square meter or pascals, and ρ is the density of the medium in kilograms per cubic meter. If this velocity is experimentally shown to be a function of the applied pressure to the medium, P, then one knows that either c is a function of pressure, ρ is a function of pressure, or both, supposing the model is inherently accurate. Assuming for the moment that stiffness c is a function of pressure and density ρ is not, then perhaps one could accurately model this pressure

response of c with a linear regression, such that:

$$c(P) = c_0 + c_1 P \tag{4.2}$$

Then for our model, it would be obvious that the coefficient c_1 is solely responsible for controlling the pressure response of stiffness, $c(P)$, and thus also the pressure response of wave velocity, $v(P)$, rather than c_0 which provides whatever value of stiffness is present at zero applied pressure. Continuing the illustration, let us assume that now in later experiments, the pressure response for velocity, $v(P)$, is found to be different when measured at a constant temperature of 25 °C then when measured at a constant temperature 75 °C. Since it was already concluded that the coefficient c_1 solely determines $v(P)$, then if $v(P)$ is found to be a function of temperature, c_1 itself *must also be a function of temperature.* In other words, if the shape of the velocity versus pressure curve experimentally changes with temperature, then the simplest way to edit the velocity model and make it agree with experiments is to make c_1 also a function of temperature that will describe the way the shape changes.

This hypothetical example can be applied to the incremental model used in the finite element analysis and laid out in Section 2.4, when the illustrative definition of stiffness in Equation (4.2) is compared to the linear stress-strain relationship for the incremental model, Equation (2.12), and specifically the incremental stiffness term (which will be referred to in this section under a single new symbol d_{ijkl}):

$$t_{ij} = (d_{ijkl}) s_{kl} \qquad \text{((2.12) recast)}$$

$$d_{ijkl} = C^{\theta}_{ijkl} + C^{\theta}_{ijklmn} S_{mn} \tag{4.3}$$

Just like c_1 in the illustration, so the third-order elastic coefficient, C^{θ}_{ijklmn}, solely controls the pressure response of the incremental stiffness through the initial strains, S_{mn}, which are direct functions of the applied pressure (as well as initial thermal strains). The incremental stiffness directly contributes to the velocity of the piezoelectrically induced thickness-shear wave, which in turn determines the overall resonant

frequency. Likewise, because C^{θ}_{ijklmn} is not in fact a function of temperature in finite element representation the incremental model (because its temperature derivatives are not known), one would expect that the pressure response of the model would be independent of temperature.

This expectation is verified in the benchmark studies regarding $\mathrm{d}K_f/\mathrm{d}T$ shown in Figure 3.9, where the change in force frequency coefficient, K_f, with respect to changing temperature is approximately zero compared to experimental values. Adding realistic temperature dependence to the 3rd-order elastic coefficients should bring about in that benchmark realistic values for $\mathrm{d}K_f/\mathrm{d}T$. Similarly in the pressure sensor model, having the temperature derivatives of 3rd-order elastic coefficients should bring the simulation's "trends of trends" into better agreement with those seen experimentally, and thereby improve the overall accuracy of the predicted frequency values when high temperatures and pressures are applied simultaneously. A proof-of-concept of this hypothesis is the subject of the next chapter.

CHAPTER 5

EXAMINING THE NEED FOR TEMPERATURE DERIVATIVES OF 3RD-ORDER ELASTIC COEFFICIENTS

5.1 Overview of the Current State

The evidence presented in the benchmark study at the end of Section 3.5 and in the pressure sensor simulation of the previous chapter highlights the need for new definitions for the constitutive properties for quartz: the temperature derivatives of the third-order elastic coefficients. The complete third-order coefficients themselves were given by Thurston, McSkimin, and Andreatch more than 45 years ago [17]. A probable reason that their temperature derivatives have not been realized after all of this time is likely a relative lack of need; while the base third-order elastic coefficients are essential to predict the frequency-stress response of a resonator, such as the frequency shift due to mounting stresses, their temperature derivatives are not generally needed (at least not for most temperatures encountered). Some current models, like Yong and Wei's total thermoelastic stiffness parameters, indirectly take into account the temperature derivatives of the nonlinear elastic terms and do adequately meet the needs of many areas of quartz research. Of course, models such as this end up making assumptions as to what states of stress and strain they can describe, and that is why they will not work for the general case where both high temperatures and high pressures may be encountered simultaneously.

That is not to say that no one has examined the independent information contained in the temperature derivatives of the third-order elastic coefficients. An interesting alternative to using the literal values in calculations is using an empirical

method involving superposition of experimental results [25]. In the referenced article, EerNisse utilizes his own experimental results for a resonator in diametric point loading in conjunction with experiments involving resonators under uniform biaxial stress to model the frequency response of a pressure sensor, which is not unlike the focus of the current work. Because the stress distribution in his pressure sensor happens to be approximated by the superposition of the point load and uniform load stress states, EerNisse was able to sum the experimental frequency shifts from each case (at a given temperature) to yield a good approximation for the overall frequency shift as a function of pressure and temperature. It is lucky for this method that the frequency-pressure response is linear, as previously demonstrated. Otherwise such superposition of frequency would not be accurate.

In the same paper, EerNisse himself acknowledges the lack of data for the temperature dependence of the third-order elastic constants. Of course, such empirical methods are inherently limited to the available cut angles, temperatures, geometries, and stress states of the primary experimental works. In any case, the empirical frequency data in and of itself is not of much use as an input in the finite element analysis. Not only, then, would experiments to obtain the needed temperature derivatives allow quartz researchers to take full advantage of the ever-progressing availability of computing power, the values would also represent the freedom to simulate completely new and untested designs with efficiency and accuracy. Furthermore, finite element algorithms like the one developed for the current work would allow the unique advantage of quick independent validation of derived values.

5.2 Pressure Response as a Function of Temperature

As a sixth-rank tensor C_{ijklmn}, the root 3rd-order elastic constants contain 3^6 or 729 numeric values used in calculations, although symmetry in the stress and strain tensors as well as energy conservation considerations dictate that many of these are

equal to each other. For this reason, it is common to represent the tensor in abbreviated engineering notation as six separate six-by-six matrices, all of which are symmetric. It is this six-by-six-by-six notation that leads to the term "third-order" in the name for C_{ijklmn}. The triclinic crystal system (the least symmetric of the seven crystal systems) has 56 independent values, while quartz exhibits such symmetry as to bring this number down to fourteen independent values [26]. (This can be compared to just six independent values of the second-order elastic coefficient of quartz, C_{ijkl}.) It follows that there are fourteen independent first temperature derivatives of C_{ijklmn}, deemed $C^{(1)}_{ijklmn}$ as previously noted in Section 2.5, and the same number of independent second temperature derivatives $C^{(2)}_{ijklmn}$.

However, because resonators typically only operate on a single mode of vibration, such as the slow thickness-shear mode for the AT-Cut pressure sensor in the current study, only one incremental stiffness term (dependent on cut angle) has primary control of the speed of the standing wave though the crystal medium, and thus controls the frequency. For the AT-Cut, this is the rotated C_{66} term as transformed to the geometric coordinate system. Therefore, for any given cut, one would expect that the entire linear temperature dependence given by the fourteen values of $C^{(1)}_{ijklmn}$ could be equivalently modeled by a single temperature-dependent scalar applied to the known 3rd-order elastic coefficients, C_{ijklmn}, because ultimately all fourteen values only effectively contribute to a single useful term, C_{66}. The actual function that maps these fourteen individual values to one scalar will not only depend on the cut angle, but also the state of initial strain. Technically, even this assumption is an approximation, because the vibration of the AT-Cut is not a pure thickness-shear mode, but a so-called "quasi-shear" mode. Thus other incremental stiffness terms besides simply C_{66} play a role in the frequency of vibration and we are not guaranteed to be able to match more than one stiffness term with single scalar.

Even so neglecting this distinction, the assumed temperature dependence of incre-

mental stiffness takes the form of the following Equation (5.1), which is used in place of Equation (2.12) in the incremental model. For this analysis, the newly-inferred temperature dependence of the third-order elastic stiffness will be assumed to not substantially change the *initial* response, so Equation (2.7) for the initial model will remain unchanged. (This assumption was verified for a single data point at 16,000 psi and 175 °C where the difference in the frequency response was less than 2 ppm.)

$$t_{ij} = (C^{\theta}_{ijkl} + C_{ijklmn}S_{mn} + C^{(1)}_{ijklmn}(S_{mn} - \alpha^{\theta}_{mn}))s_{kl} \tag{5.1}$$

$$C^{(1)}_{ijklmn} = \gamma \cdot \theta \cdot C_{ijklmn} \tag{5.2}$$

Where γ (gamma) is an assumed scalar constant with units of $^{\circ}\mathrm{C}^{-1}$ and θ is the change in temperature from reference, $T - T_{ref}$ in °C. The expression "$(S_{mn} - \alpha^{\theta}_{mn})$" which is the difference between the total strain and the thermal strain, is used to approximate the elastic portion of total strain (as opposed to the thermal expansion portion, α^{θ}_{mn}). This distinction is necessary in order to leave the previous definition of $\tilde{C}^{(2)}_{ijkl}$ and $\tilde{C}^{(3)}_{ijkl}$ within C^{θ}_{ijkl} intact in their current theoretical form with given numerical values. As previously explained in Section 2.5 with Equations (2.24) and (2.25), this definition dictates that the derived values of these 'effective' temperature derivatives already include the thermal strain contribution of the temperature derivatives of the third-order elastic stiffness, and so the current expression with γ needs only apply to the elastic strains, or those caused by the reaction to stresses. The idea that the elastic strain and thermal strain parts can be simply pulled out of the total strains involves the assumption that nonlinear (large deformation) strain terms are negligible for this case.

In order to calibrate a realistic value of the constant γ (gamma) for the AT-Cut sensor of the current work, a sensitivity study was performed with the goal of using γ to improve a single aspect of the otherwise standard pressure sensor simulation, which was explained in the previous chapter. This aspect was the isobaric tempera-

ture versus frequency response at 16,000 psi. In order to accelerate this fact-finding mission, only three temperature points where taken at 25 °C, 50 °C, and 175 °C. The logic behind this unbalanced distribution was to take 25 °C to prove that the reference temperature response would remain unchanged, then to take a high temperature and a low temperature other than 25 °C. The results are given alongside experimental values in Figure 5.1.

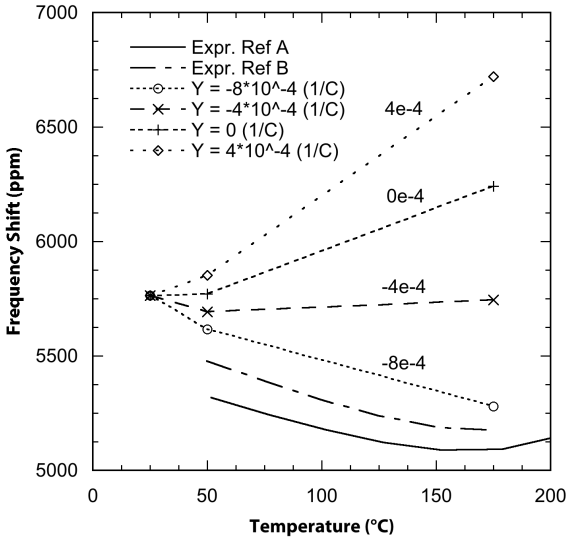

Figure 5.1: Sensitivity study for 3rd-order elastic scalar temperature constant

As seen in Figure 5.1, it appears that a value for the scalar temperature constant, γ, that most nearly creates the same trend in the simulation as seen experimentally would be about $\gamma \approx -7.75 \times 10^{-4}$. This assessment neglects the small vertical offset of the simulation's values and concentrates on the overall shape and slope of the plot. With this predicted value for γ in hand, it can now be used to rerun the frequency response of the entire temperature and pressure input range. The expectation being that applying the γ value which was tuned to benefit only one part of the model would actually increase the accuracy of the frequency response throughout for this certain case; namely for AT-Cut quartz and relative strain distribution unique to the particular pressure sensor studied. The results of this trial are presented in the follow-

ing section. All factors are the same as the sensor simulation in the previous chapter except the new definition for third-order elastic coefficients given in Equation (5.2).

5.3 Modified Sensor Model Results

Similar to the presentation of the results of the simulation in the previous chapter, the isobaric and isothermal slices of this surface are given in Figure 5.3 and Figure 5.2, respectively. The referenced experimental data is the same as the previous chapter. The error of the simulation compared to experimental values, as previously described at certain high-pressure points, was for this modified model 4.83% at 50 °C and 20,000 psi and then actually was slightly reduced with temperature to 3.97% at 200 °C and 20,000 psi.

5.4 Conclusions

Overall, one can easily see the improvement from the results of the previous chapter at high temperatures and pressures. For example, the percent error of the modified model relative to the experimental values at the two 20,000 psi points previously reported (4.83% at 50 °C and 3.97% at 200 °C) was much less than the unmodified model of the previous chapter, which yielded error values at the same points of 7.52% and 25.65%, respectively. Comparing the low-pressure isobaric plots between the modified model and the previous chapter (Figures 4.3(a) and 5.3(a)), one can see that there is not much change in the temperature response at, for instance, 14 psi. Similarly, the low-temperature isothermal plots agree well with experimental values in both cases, and so do not show much change between the modified and unmodified models.

Looking at the form of the assumed temperature dependence of modified third-order elastic constants in Equation (5.1), this lack of change in the frequency response at low temperature or pressure is predicted. The modified term contains the expres-

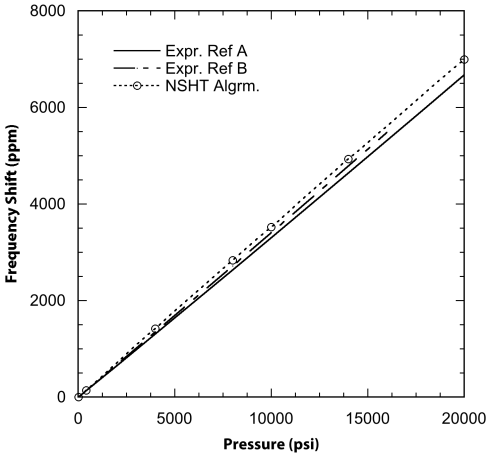

(a) T = 50 °C

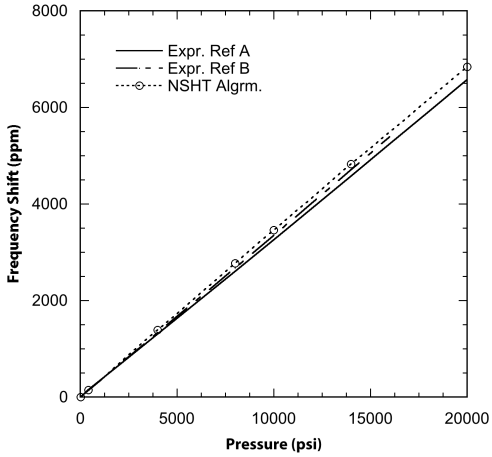

(b) T = 75 °C

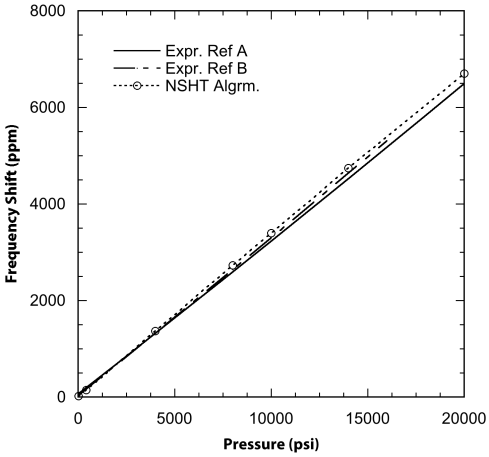

(c) T = 100 °C

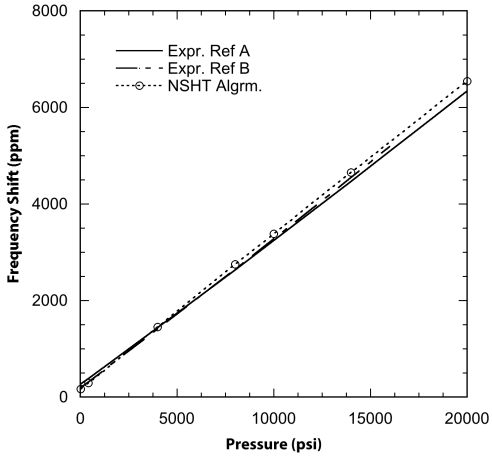

(d) T = 150 °C

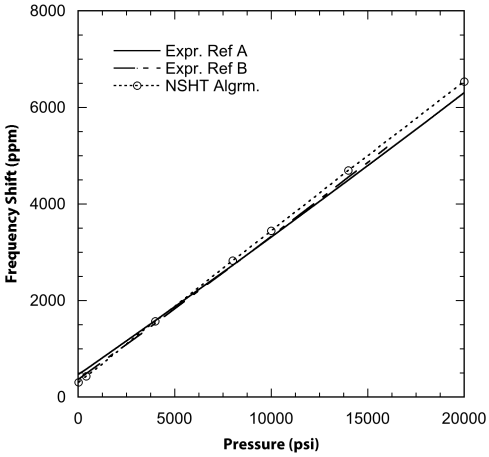

(e) T = 175 °C

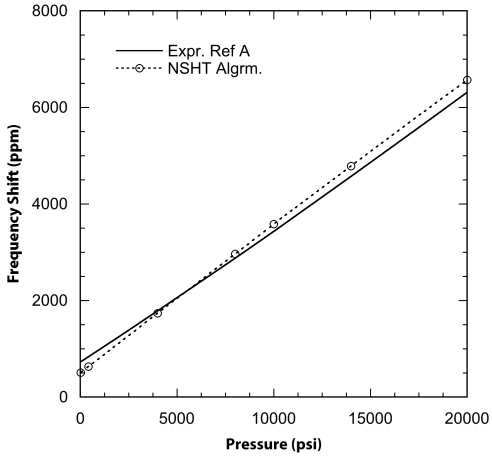

(f) T = 200 °C

Figure 5.2: Modified isothermal frequency-pressure sensor response

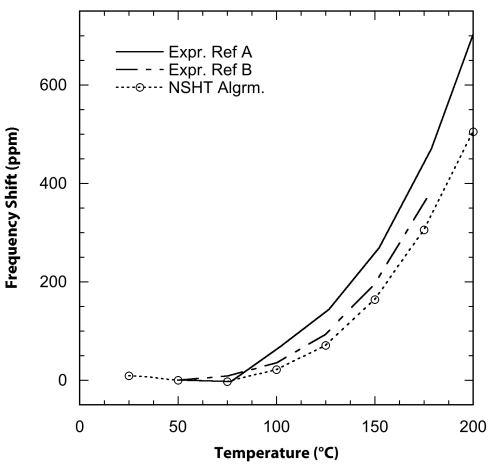

(a) P = 14 psi

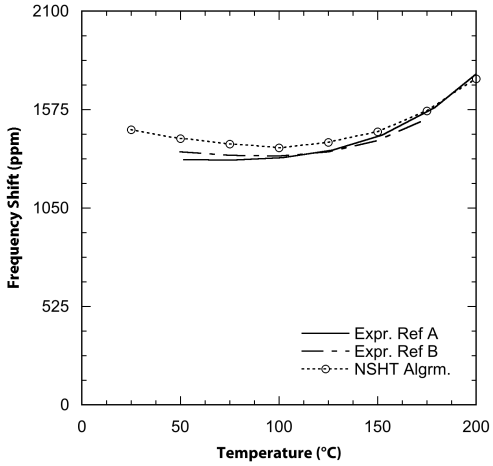

(b) P = 4,000 psi

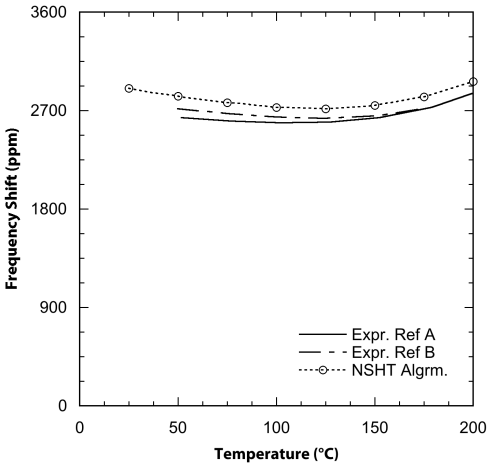

(c) P = 8,000 psi

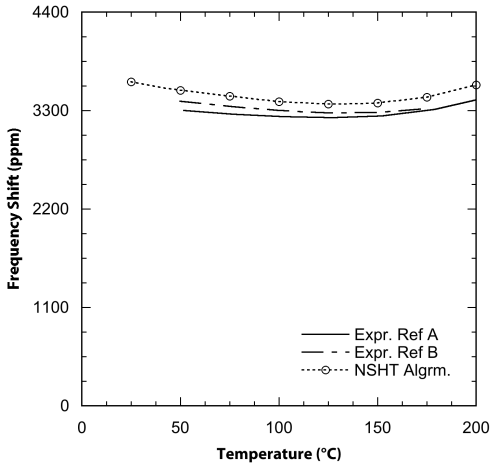

(d) P = 10,000 psi

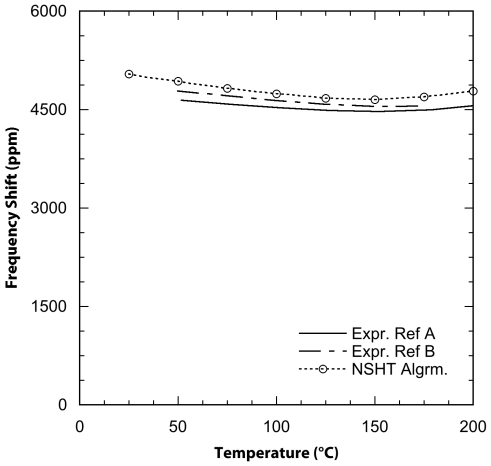

(e) P = 14,000 psi

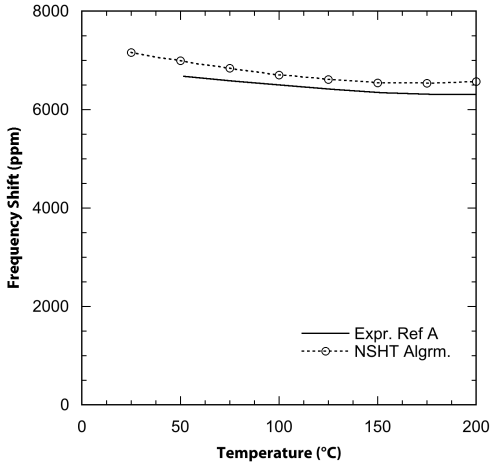

(f) P = 20,000 psi

Figure 5.3: Modified isobaric frequency-temperature sensor response

sion "$S_{mn} - \alpha^{\theta}_{mn}$" which was used to approximate the elastic portion of the total strains as previously described. Because at low pressure, the elastic strains are negligible compared to the thermal strains, then this term is approximately zero, and the modification has no effect. Similarly, at low temperatures near the reference at 25 °C, the relative temperature term θ will be small as applied in Equation (5.2), again demoting the impact of the modification. The result is that the modification really only applies to high temperatures and high pressures, which happened to be where the unmodified model was weakest.

This is an important distinction: the form of the modification was not at all based on any experimental trends, except in assigning a numeric value to γ. In other words, the modification to the incremental constitutive equation itself was not an attempt to 'curve fit' the overall results. Rather, it was derived using the equations of thermoelasticity from an assumed linear temperature response of the third-order elastic constants, which was the simplest augmentation to their previous temperature independent state, while also taking into account that the 'effective' second-order temperature derivatives already contained part of this information. Therefore, the fact that this analytically-derived modification (with a single empirically-derived parameter) can improve the response of the entire model indicates that the temperature response of the third-order elastic constants is important to the accuracy of the predicted frequency for high temperatures and pressures.

The value of γ itself is not meant to be important, as its use for predicting the response has essentially the same limitations as EerNisse's empirical analysis previously described. What is important is its validation of the hypothesis that incorporating thermally-induced changes in the third-order elastic coefficients will visibly increase the accuracy of some quartz simulations, such as in this case, the high-temperature pressure sensor. The fact that a single value of γ performs well in this role is a testament to the order and consistency of the underlying temperature derivatives of the

third-order elastic stiffness. Indeed, a complete set of such derivatives would allow an increase in accuracy, similar to the one attained in this chapter, for any cut angle, geometry, or state of strain. Of course, the need for this accuracy is dependent on the application of the simulation, where studies involving high temperatures and high pressures simultaneously will tend to see the most benefit.

CHAPTER 6

FUTURE WORK

6.1 Deriving the Temperature Derivatives of Third-Order Elastic Stiffness of Quartz

Having laid out the need for and potential benefits of the yet unpublished temperature derivatives of third-order elastic stiffness of α-quartz, an obvious avenue for future work would be to experimentally derive these fourteen independent values for each of the first and second temperature derivative tensors. The work of Thurston, McSkimin, and Andeatch [17] on the third-order elastic constants at reference temperature seems to have held up well in the studies of the past 45 years, so one option would be to repeat their work at varied temperatures. Their method utilizes the measured transit time of small-amplitude ultrasonic waves as a function of applied hydrostatic and uniaxial stress. From this raw data, the third-order values can be calculated using relations given by Brugger [27] and a least squares fit.

As an alternative to this direct approach, or perhaps as a preliminary estimation, one could instead opt to reanalyze data from appropriate previously published work. One such work that seems to be rich in information from the temperature response of third-order elastic coefficients is that used in the current benchmark studies by EerNisse [21], which also included original data from Dauwalter [22]. This study defined the linear temperature dependence of the "force frequency coefficient" K_f for various cuts of quartz, although K_f is not strictly a material property itself in a thermoelastic sense, but more of an empirical curve fit parameter for the frequency versus diametric load response. The classic elasticity solution for the 'disk in diametric com-

pression' geometry associated with K_f could be used to estimate the state of strain, although such a study would be better served by the equivalent anisotropic analytical solution given by Janiaud, Nissim, and Gagnepain [28], which of course would be more directly applicable for quartz. From this analytic initial response, the experimental frequency change could be related to the unknown temperature derivatives via the incremental piezoelectric equations using a perturbation analysis technique [29][30], which was previously used for other quartz properties by Lee and Yong [12] and Yong and Wei [11]. It may be that there are not enough independent orientations of the crystal relative to the applied stress to glean all fourteen independent values from EerNisse's data, so it is possible that one would still have to do more experiments to get the full set, or otherwise look elsewhere for extra constraining data.

A third option for deriving the temperature derivatives of third-order elastic constants would be numeric curve fitting by repetitively using assumed values of the fourteen derivatives within a simulation such as the finite element algorithms developed in the current work. Such an undertaking could be very similar to the method used to find the assumed temperature scalar γ in the previous chapter, but on a much larger scale. This approach has an advantage over the perturbation method in that the state of strain need not be analytically solved, since it can be numerically derived within the simulation. Thus, experimental data like EerNisse's could be coupled with completely unrelated data, such as the experimental frequency response of the pressure sensor, in order to develop a more complete picture of the temperature derivatives as seen from every angle. Of course, a major determining factor in the feasibility of this approach would be the accessibility of the vast computing power needed to perform the repetitive analysis in a somewhat timely manner. With some two independent variable sweeps taking on the order of 35 hours, one would likely want substantially more clout than the dual-chip 2.8GHz Intel Quad-Core Xeon desktop system, which was used in (and adequate for) the current study.

6.2 Applied Simulations

Even without the desired temperature derivatives, the model without temperature dependence of the third-order elastic coefficients will be useful for future work, based on the results of Chapter 4. Testing of new sensor design parameters such as cut angle and geometry would definitely be assisted by a simulation like the one developed. The model's response of frequency versus temperature and pressure, even without the temperature derivatives of third-order elasticity, is definitely accurate enough to get a sense of sensitivity trends as functions of design changes. Investigating the modeled response of the various harmonic overtone modes of the quartz resonator could also lend insight to sensor improvements. Of course, if the temperature derivatives of the third-order elastic coefficients were known, these applied simulations would be all the more acute.

A major asset of the finite element method used in this study is its versatility. Although the algorithms here developed concentrate on the use of quartz as temperature and pressure sensors for the oil and gas industry, quartz can be utilized in many other extreme conditions, such as aerospace sensory and frequency control applications. The method described owes its flexibility to the fact that the inputs are elementary and tied to the material composition itself, so that wherever the material is used, an accurate finite element model should find use as well. Modeling the coupled electrical and mechanical phenomena of piezoelectric materials can also serve as a foundation to investigate the framework of other couplings present in nature, such as mechanical-chemical couplings in biosystems, or thermo-electrical coupling in power transmission. That is, the idea of putting the proven separate models together with some known coupling term that is present in each system, like the piezoelectric tensor in this case, can help tie together the underpinning theories of applied research in ways that reflect the true complex reactions of reality.

BIBLIOGRAPHY

[1] W. G. Cady, *Piezoelectricity; an introduction to the theory and applications of electromechanical phenomena in crystals*. International series in pure and applied physics, New York, London,: McGraw-Hill Book Company, inc., 1st ed., 1946.

[2] V. E. Bottom, *Introduction to quartz crystal unit design*. Van Nostrand Reinhold electrical/computer science and engineering series, New York: Van Nostrand Reinhold, 1982.

[3] J. D. Dana and W. E. Ford, *Dana's manual of mineralogy for the student of elementary mineralogy, the mining engineer, the geologist, the prosepctor, the collector, etc.* New York,: J. Willey & sons; etc., 13th ed., 1912.

[4] V. E. Bottom, "A history of the quartz crystal industry in the usa," in *Thirty Fifth Annual Frequency Control Symposium. 1981*, pp. 3–12, 1981.

[5] "Ieee standard on piezoelectricity," *ANSI/IEEE Std 176-1987*, pp. 16, 5, 7, 1988.

[6] "Standards on piezoelectric crystals, 1949," *Proceedings of the IRE*, vol. 37, no. 12, pp. 1378–1395, 1949.

[7] T. R. Meeker, "A review of the new ieee standard on piezoelectricity," in *33rd Annual Symposium on Frequency Control. 1979*, pp. 176–180, 1979.

[8] M. H. Sadd, *Elasticity : theory, applications, and numerics*. Amsterdam ; Boston: Elsevier/AP, 2nd ed., 2009.

[9] L. E. Malvern, *Introduction to the mechanics of a continuous medium*. Prentice-Hall series in engineering of the physical sciences, Englewood Cliffs, N.J.,: Prentice-Hall, 1969.

[10] P. C. Y. Lee and Y. K. Yong, "Temperature derivatives of elastic stiffness derived from the frequency-temperature behavior of quartz plates," *Journal of Applied Physics*, vol. 56, no. 5, pp. 1514–1521, 1984.

[11] Y.-K. Yong and W. Wei, "Lagrangian temperature coefficients of the piezoelectric stress constants and dielectric permittivity of quartz," in *Frequency Control Symposium and Exhibition, 2000. Proceedings of the 2000 IEEE/EIA International*, pp. 364–372, 2000.

[12] P. C. Y. Lee and Y. K. Yong, "Frequency-temperature behavior of thickness vibrations of doubly rotated quartz plates affected by plate dimensions and orientations," *Journal of Applied Physics*, vol. 60, no. 7, pp. 2327–2342, 1986.

[13] P. C. Y. Lee and Y. K. Yong, "Frequency-temperature behavior of thickness vibrations of doubly-rotated quartz plates affected by plate dimensions and orientations," in *38th Annual Symposium on Frequency Control. 1984*, pp. 164–175, 1984.

[14] M. S. Patel, *Nonlinear Behavior in Quartz Resonators and its Stability*. Ph.d. dissertation, Rutgers, The State University of New Jersey, 2008.

[15] K. Brugger, "Thermodynamic definition of higher order elastic coefficients," *Physical Review a-General Physics*, vol. 133, no. 6A, pp. 1611–1612, 1964.

[16] R. Bechmann, A. D. Ballato, and T. J. Lukaszek, "Higher-order temperature coefficients of the elastic stiffinesses and compliances of alpha-quartz," *Proceedings of the IRE*, vol. 50, no. 8, pp. 1812–1822, 1962.

[17] R. N. Thurston, H. J. McSkimin, and P. Andreatch, "Third-order elastic coefficients of quartz," *Journal of Applied Physics*, vol. 37, no. 1, pp. 267–275, 1966.

[18] R. Bechmann, "Elastic and piezoelectric constants of alpha-quartz," *Physical Review*, vol. 110, no. 5, p. 1060, 1958.

[19] T. R. Chandrupatla and A. D. Belegundu, *Introduction to finite elements in engineering*. Upper Saddle River, N.J.: Prentice Hall, 3rd ed., 2002.

[20] E. P. EerNisse, "Quartz resonator frequency shifts arising from electrode stress," in *29th Annual Symposium on Frequency Control. 1975*, pp. 1–4, 1975.

[21] E. P. EerNisse, "Temperature dependence of the force frequency effect for the at-, fc-, sc-, and rotated x-cuts," in *34th Annual Symposium on Frequency Control. 1980*, pp. 426–430, 1980.

[22] C. R. Dauwalter, "The temperature dependence of the force sensitivity of at-cut quartz crystals," in *26th Annual Symposium on Frequency Control. 1972*, pp. 108–112, 1972.

[23] G. R. Kirikera, W. Patton, and S. Behr, "Modeling thickness shear mode quartz sensors for increased downhole pressure and temperature applications," in *COMSOL Conference 2010*, 2010.

[24] E. P. EerNisse and R. B. Wiggins, "Review of thickness-shear mode quartz resonator sensors for temperature and pressure," *Sensors Journal, IEEE*, vol. 1, no. 1, pp. 79–87, 2001.

[25] E. P. EerNisse, "Theoretical modeling of quartz resonator pressure transducers," in *41st Annual Symposium on Frequency Control. 1987*, pp. 339–343, 1987.

[26] K. Brugger, "Pure modes for elastic waves in crystals," *Journal of Applied Physics*, vol. 36, no. 3, pp. 759–768, 1965.

[27] K. Brugger, "Determination of third-order elastic coefficients in crystals," *Journal of Applied Physics*, vol. 36, no. 3, pp. 768–773, 1965.

[28] D. Janiaud, L. Nissim, and J. J. Gagnepain, "Analytical calculation of initial stress effects on anisotropic crystals: Application to quartz resonators," in *32nd Annual Symposium on Frequency Control. 1978*, pp. 169–179, 1978.

[29] H. F. Tiersten, "Perturbation-theory for linear electroelastic equations for small fields superposed on a bias," *Journal of the Acoustical Society of America*, vol. 64, no. 3, pp. 832–837, 1978.

[30] A. H. Nayfeh, "Numerical-perturbation methods in mechanics," *Computers and Structures*, vol. 30, no. 1-2, pp. 185–204, 1988.

[31] T. L. Anderson, R. E. Newnham, and L. E. Cross, "Coercive stress for ferrobielastic twinning in quartz," in *31st Annual Symposium on Frequency Control. 1977*, pp. 171–177, 1977.

[32] L. D. Clayton and E. P. Eernisse, "Application of finite element analysis to the design of quartz thickness-shear mode pressure sensors," in *Proceedings of the 50th Annual IEEE International Frequency Control Symposium, 1996*, pp. 541–549, 1996.

VITA

Austin Dale Beerwinkle

Candidate for the Degree of

Master of Science

Thesis: NONLINEAR FINITE ELEMENT MODELING OF QUARTZ CRYSTAL RESONATORS

Major Field: Mechanical and Aerospace Engineering

Biographical:

Personal Data: Born in Oklahoma, USA in 1986.

Education:

Received the B.S. degree from Oklahoma State University, Stillwater, OK, USA, 2009, in Aerospace and Mechanical Engineering

Completed the requirements for the degree of Master of Science with a major in Mechanical and Aerospace Engineering at Oklahoma State University in July, 2011.

Experience:

Member of Technical Staff at Sandia National Laboratories, Albuquerque, NM, USA

Graduate Research Assistant at the Mechanics of Advanced Materials Laboratory under Dr. Raman P. Singh

Engineering Intern at Spirit Aerosystems, Tulsa, OK, USA

Engineering Intern at General Electric Aviation, Arkansas City, KS, USA

Engineering Intern at AGCO Corporation, Hesston, KS, USA

Name: Austin Dale Beerwinkle Date of Degree: July, 2011

Institution: Oklahoma State University Location: Stillwater, Oklahoma

Title of Study: NONLINEAR FINITE ELEMENT MODELING OF QUARTZ CRYSTAL RESONATORS

Pages in Study: 69 Candidate for the Degree of Master of Science

Major Field: Mechanical and Aerospace Engineering

In order to facilitate the design of quartz resonators, the overall goal of the current work was to develop an accurate three-dimensional finite element model for the anisotropic frequency response of quartz. The model was based on the linear incremental equations for superimposed small vibrations onto nonlinear thermoelastic stressed media. The frequency response of the model was benchmarked to experimental data from quartz pressure sensors with temperature ranging from 50 °C to 200 °C and pressure from 14 psi to 20,000 psi. This direct finite element approach for frequency response at such high pressure had not been previously examined in literature.

The normalized frequency response to the change in external pressure from 14 psi to 20,000 psi matched very well with experimental data for lower temperatures, having a maximum deviation of only 7.5% at 20,000 psi when assuming constant 50 °C temperature. However, the same deviation grew to 25.7% assuming a higher 200 °C constant temperature. Similarly, the temperature-frequency response at constant pressure from 50 °C to 200 °C matched the experimental trend well for lower pressures, but this agreement deteriorated as pressure increased.

The nature of the observed frequency deviations suggests that changes in the third-order elastic constants with temperature, a quartz material definition that is not currently available in literature, could play a significant role in accurately modeling the frequency response at such conditions, and that the lack of such properties is the primary source of the error in both temperature and pressure response. This hypothesis was tested by using a novel method of giving the third-order elastic constants linear temperature dependence based on a single scalar parameter, for which a specific value was empirically derived for the AT-Cut quartz pressure sensor studied. Specifically, modeling a scalar decrease in magnitude of about 0.0775% per °C in the third-order elastic coefficients was shown to decrease the error of the simulation at the highest temperature and pressure from 25.7% to 4.0%, and this improvement was mirrored throughout the range of temperatures and pressures tested. Furthermore, knowing the expected benefit of implementing the third-order elastic coefficients as functions of temperature should aid future researchers in deciding if defining their full anisotropic temperature derivatives is practical, and relevant possibilities for such a study are given.

ADVISOR'S APPROVAL: _____